Geoscience Frontiers 10 (2019) 1507–1520

HOSTED BY

Contents lists available at ScienceDirect

China University of Geosciences (Beijing)

Geoscience Frontiers

journal homepage: www.elsevier.com/locate/gsf

Research Paper

Petrogenesis and tectonic implications of Early Cretaceous andesitic–dacitic rocks, western Qinling (Central China): Geochronological and geochemical constraints

Feifei Zhang [a,*], Peter A. Cawood [b,c], Yunpeng Dong [a], Yuejun Wang [d]

[a] State Key Laboratory of Continental Dynamics, Department of Geology, Northwest University, Xi'an 710069, China
[b] Department of Earth Sciences, University of St. Andrews, North Street, St. Andrews KY16 9AL, UK
[c] School of Earth, Atmosphere and Environment, Monash University, Melbourne, Victoria 3800, Australia
[d] Guangdong Provincial Key Lab of Geodynamics and Geohazards, School of Earth Sciences and Engineering, Sun Yat-sen University, Guangzhou 510275, China

ARTICLE INFO

Article history:
Received 30 September 2017
Received in revised form
19 June 2018
Accepted 27 September 2018
Available online 27 November 2018
Handling Editor: M. Santosh

Keywords:
$^{40}Ar/^{39}Ar$ and zircon U–Pb geochronology
Sr–Nd isotopes
Early Cretaceous
AFC process
Continental lithospheric mantle
Western Qinling orogenic belt

ABSTRACT

$^{40}Ar/^{39}Ar$ and zircon U–Pb geochronological and whole-rock geochemical analyses for the Laozanggou intermediate-acidic volcanic rocks from the western Qinling orogenic belt, Central China, constrain their petrogenesis and the nature of the Late Mesozoic lithospheric mantle. These volcanic rocks yield hornblende or whole-rock $^{40}Ar/^{39}Ar$ plateau ages of 128.3–129.7 Ma and zircon U–Pb age of 131.3 ± 1.3 Ma. They exhibit SiO_2 of 56.86–66.86 wt.%, K_2O of 0.99–2.46 wt.% and MgO of 1.03–4.47 wt.%, with Mg# of 42–56. They are characterized by arc-like geochemical signatures with significant enrichment in LILE and LREE and depletion in HFSE. All the samples have enriched Sr–Nd isotopic compositions with initial $^{87}Sr/^{86}Sr$ ratios ranging from 0.7112 to 0.7149 and $\varepsilon_{Nd}(t)$ values from −10.2 to −6.3. Such geochemical signatures suggest that these volcanic rocks were derived from enriched lithosphere-derived magma followed by the assimilation and fractional crystallization (AFC) process. The generation of the enriched lithospheric mantle is likely related to the modification of sediment-derived fluid in response to the Triassic subduction/collision event in Qinling orogenic belt. The early Cretaceous detachment of the lithospheric root provides a reasonable mechanism for understanding the petrogenesis of the Laozanggou volcanic sequence in the western Qinling orogenic belt.

1. Introduction

Calc-alkaline andesitic and dacitic volcanic rocks are key carriers for probing the tectonic evolution of convergent plate margins and are crucial rocks for better understanding continental crustal evolution (Boettcher, 1973; Miyashiro, 1974; Gill, 1981; Grove and Kinzler, 1986; Wilson, 1989; Davies and Stevenson, 1992; Poli and Schmidt, 2002; Ernst, 2010; Cawood et al., 2013; Shellnutt et al., 2014). The formation of subduction-related andesites and dacites is considered to be related to either partial melting of a pyroxenitic mantle or mixing of subducted oceanic crust- and overlying wedge-derived magma, with potential crustal contamination en route (e.g., Hawkesworth et al., 1993; Pearce and Peate, 1995; Kelemen et al., 2003; Rudnick and Gao, 2003; Zellmer et al., 2005; Tatsumi, 2006; Lee et al., 2007; Reubi and Blundy, 2009; Chiaradia et al., 2011; Till et al., 2012). However, the generation mechanism of the calc-alkaline andesites–dacites in intracontinental settings is still unclear, and thus the origin of early Cretaceous andesitic rocks in the Qinling orogenic belt constitutes the focus of this paper.

The Qinling orogenic belt was formed as a result of the multi-phase subduction and continental–continental collision between the North China Craton and the South China Block, and is usually subdivided into two parts: the eastern and western Qinling orogenic belts (e.g., Hacker et al., 1998; Jahn et al., 1999; Meng and Zhang, 2000; Zhang et al., 2001; Ayers et al., 2002; Li et al., 2002a; Bryant et al., 2004; Zheng, 2008; Dong et al., 2011a,b). Final collisional assembly of North and South China occured in late Triassic, at which time the Qinling orogenic belt entered an intracontinental mountain-building regime. Our work, along with other related data (Feng et al., 2003), documents the volcanic-sedimentary sequence of the late Mesozoic continental-facies andesitic–dacitic rocks in the Laozanggou area of the western

* Corresponding author.
E-mail address: zhangff@nwu.edu.cn (F. Zhang).
Peer-review under responsibility of China University of Geosciences (Beijing).

https://doi.org/10.1016/j.gsf.2018.09.013

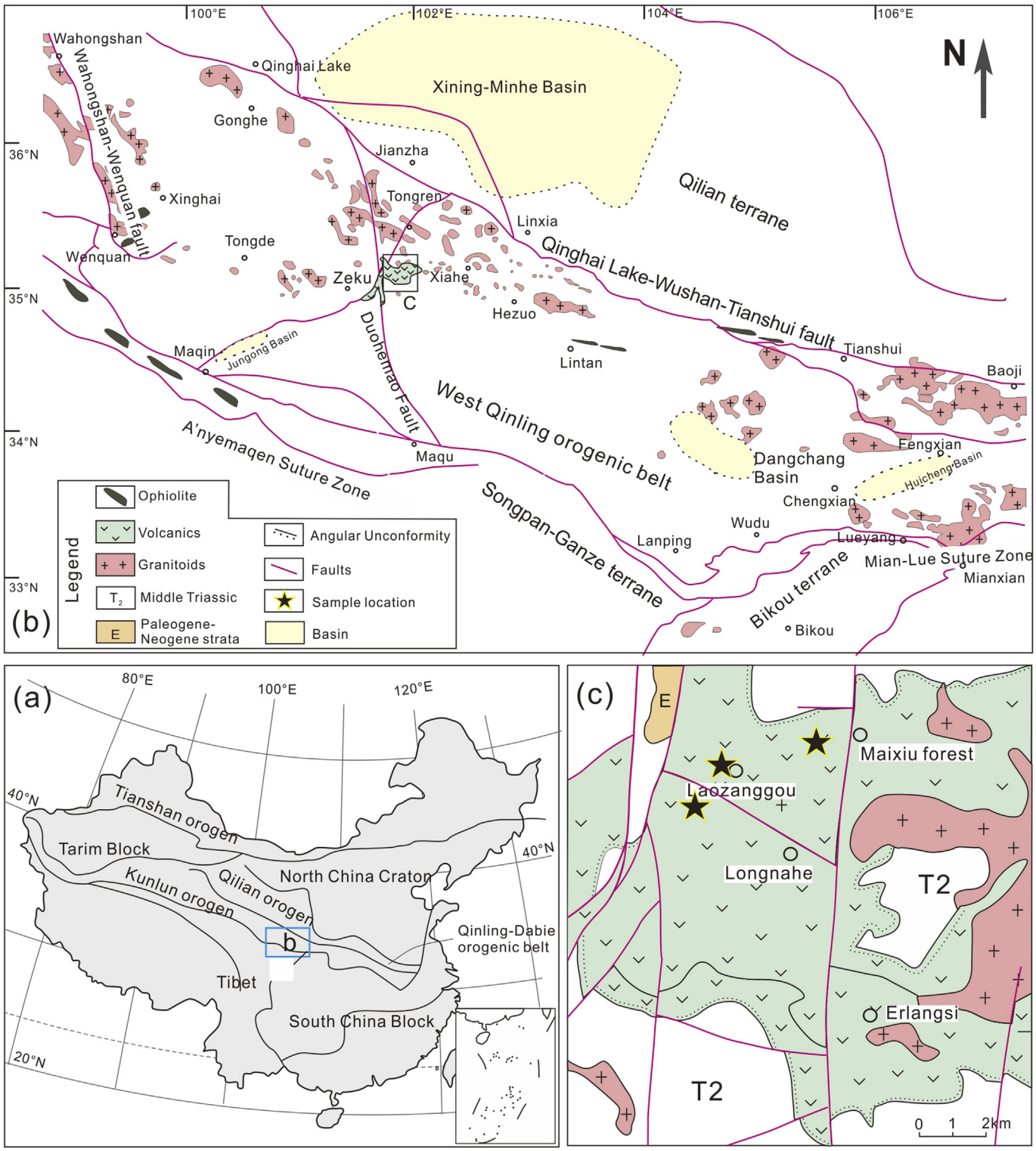

Figure 1. (a) Simplified geological map of the major tectonic units in China showing the Qinling orogenic belt (Zheng et al., 2009; Dong et al., 2011a). (b) Schematic map showing major tectonic units for the western Qinling orogenic belt (modified after Feng et al., 2002; Zhang et al., 2006). (c) Geological map showing the early Cretaceous Laozanggou volcanic sequence.

Qinling orogenic belt. This paper presents a set of new whole-rock major oxides and trace elemental data, and the $^{40}Ar/^{39}Ar$ and zircon U–Pb geochronological results for these andesitic–dacitic rocks to understand their petrogenesis and source, and to constrain their geodynamic setting.

2. Geological setting and petrography

The Qinling orogenic belt is a complex evolution extending from the Proterozoic to the Mesozoic (Fig. 1; e.g., Zhang et al., 1989, 1995a,b, 1996, 2001; Meng and Zhang, 2000; Dong et al., 2011b,

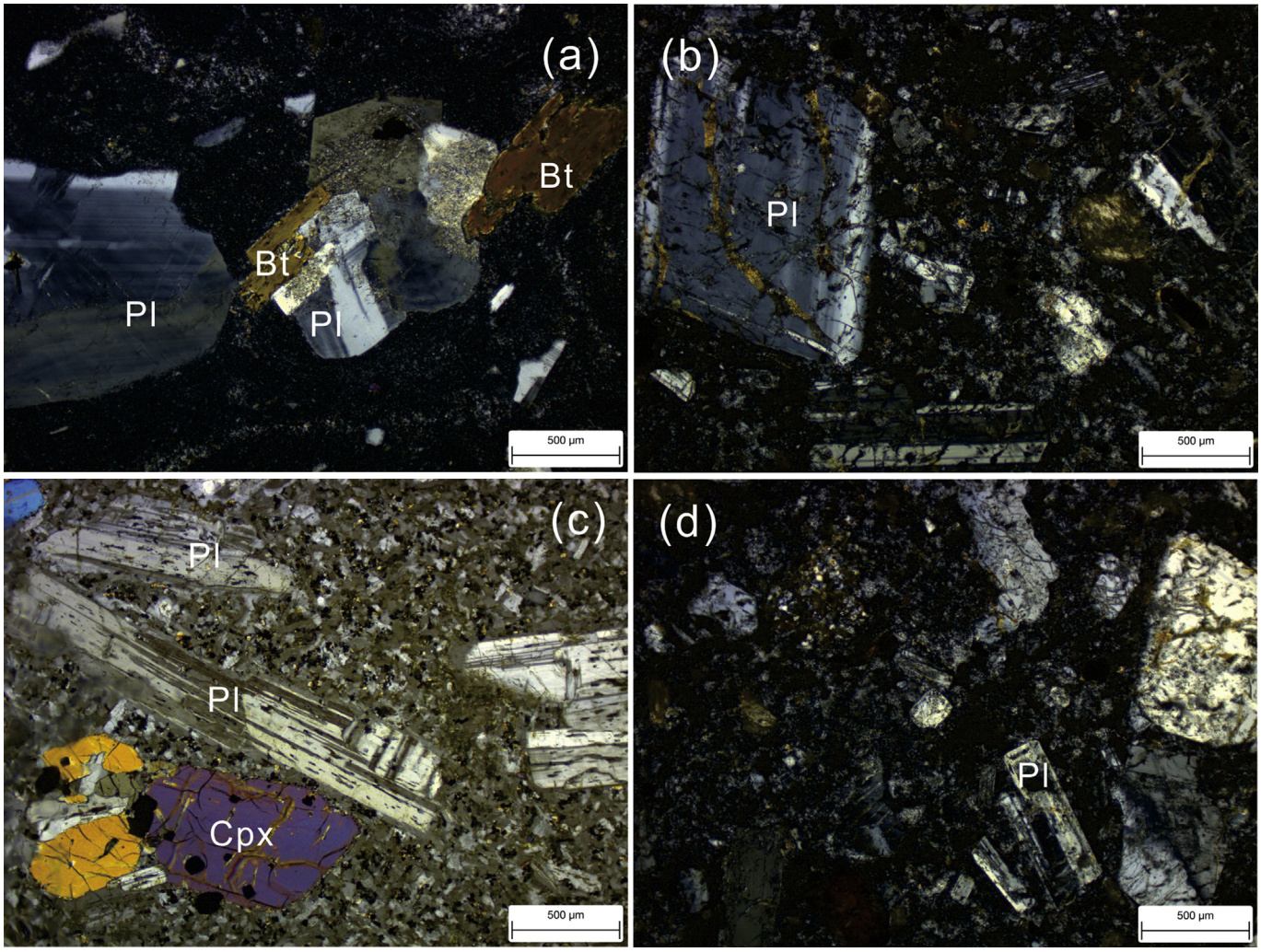

Figure 2. Representative photomicrographs for the Laozanggou andesitic (a–c) and dacitic (d) samples of the Duofutun Group in the western Qinling orogenic belt. Abbreviation: Pl–plagioclase, Cpx–clinopyroxene, Bt–biotite.

2016). The Paleozoic and early Mesozoic tectonic patterns of this orogenic belt have been well documented, which are characterized by the early Paleozoic and Triassic subduction and subsequent collision along the Shangdan and A'nyemaqen–Mianlue suture zones (e.g., Mattauer et al., 1985; Sengör, 1985; Enkin et al., 1992; Kröner et al., 1993; Li et al., 1993, 1996; Okay and Sengör, 1993; Zhang et al., 1995a,b, 1996, 2001; Ames et al., 1996; Hacker et al., 1998; Zhai et al., 1998; Meng and Zhang, 2000; Dong et al., 2004, 2011a,b, 2016, 2017). Triassic collision resulted in fold-and-thrust deformation and felsic magmatism along the Qinling orogenic belt, and corresponds with the final amalgamation of the North China Craton with South China Block (e.g., Zhang et al., 1995a,b, 1996, 2000, 2001; Meng and Zhang, 2000; Feng et al., 2002). Following the final collision, the Qinling orogenic belt lay in an intracontinental setting (Zhang et al., 2001; Dong et al., 2016).

The Qinling orogenic belt is divided into the eastern and western Qinling orogenic belts by the Fengxian-Taibai strike-slip shear zone and the Huicheng Basin (e.g., Zhang et al., 2004; Zheng et al., 2009). The western Qinling orogenic belt is separated from the Qilian terrane to the north by the Qinghai Lake–Wushan–Tianshui suture zone, from the East Kunlun orogenic belt to the west by the Wahongshan-Wenquan fault, and from the Songpan-Ganzi terrane to the south by the A'nyemaqen and Mian-Lue suture zones (Fig. 1a,b; e.g., Feng et al., 2003; Zhang et al., 2004; Meng et al., 2005; Dong et al., 2011a; Li et al., 2013a,b). The western Qinling is interpreted to be a micro-continental block that originally split from the North China Craton, and migrated southwards during the Meso- and Neoproterozoic, and then was united with the North China with South China blocks during the Triassic collision (e.g., Meng et al., 2005; Zheng et al., 2009; Dong et al., 2011a).

In the western Qinling orogenic belt, the oldest exposed crystalline basement is the Qinling Group, which includes Neoarchean gneisses, amphibolites and marble (e.g., Dong et al., 2011a). The Phanerozoic sedimentary package is subdivided into the lower Paleozoic, upper Paleozoic and the middle Jurassic–lower Cretaceous sequences across three regional angular unconformities (e.g., Qinghai Bureau of Geology and Mineral Resources (Qinghai BGMR), 1991; Wu et al., 2014). The Paleozoic rocks are dominated by shallow-marine sandstone, siltstone, argillaceous slate, shale, limestone and brecciated limestone with the exception of Silurian and Upper Devonian deep-marine siliciclastic rocks. The Triassic sequence is composed of siliciclastic and carbonate deep-marine deposits, which are considered to have accumulated in a continental slope environment (Meng et al., 2007). The middle Triassic sequence is characterized by siliciclastic rocks, and is uncomfortably overlain by upper Cretaceous sandstone in the Laozanggou area (Fig. 1c). The Jurassic–Cretaceous and Cenozoic red-bed sequences are mainly deposited in alluvial and fluvial environment of

Table 1
$^{40}Ar/^{39}Ar$ isotopic results of the incremental heating experiments for the representative andesitic–dacitic samples from the western Qinling orogenic belt.

Temp. (°C)	$(^{40}Ar/^{39}Ar)_m$	$(^{36}Ar/^{39}Ar)_m$	$(^{37}Ar/^{39}Ar)_m$	$(^{38}Ar/^{39}Ar)_m$	$^{39}Ar_k$ (10^{-12} mol)	$(^{40}Ar^*/^{39}Ar)_k$	±1σ	$^{39}Ar_k$ (%)	Apparent age (Ma)	±1σ
TR-30 Hornblende, $J = 0.0137712$										
900	9.322	0.0168	9.4521	0.0212	0.011	5.283	4.400	2.73	126.7	106.61
950	9.042	0.0226	30.850	0.0644	0.003	5.444	13.76	2.67	130.4	16.9
1000	6.570	0.0055	1.9926	0.0047	0.113	5.145	0.410	29.02	123.5	9.9
1050	6.682	0.0070	6.4658	0.0152	0.035	5.258	1.320	27.13	126.1	7.9
1100	6.615	0.0059	7.4411	0.0091	0.069	5.611	0.650	17.13	134.3	15.7
1200	6.786	0.0099	19.820	0.0291	0.025	5.860	1.820	19.13	140.0	19.4
1300	10.05	0.0367	66.145	0.2634	0.002	5.868	24.00	1.08	140.2	17.5
1350	9.725	0.0491	108.98	0.4032	0.001	6.259	43.79	1.07	149.2	80.8
Plateau age: 128.3 ± 14.9 Ma; Sample mass: 200 mg										
TR-50 whole rock, $J = 0.0137687$										
300	9.201	0.0138	1.1370	0.0235	0.101	5.236	0.460	1.47	125.6	11.0
500	7.656	0.0089	1.2774	0.0178	0.198	5.142	0.230	2.89	123.4	5.7
620	8.399	0.0098	0.6548	0.0091	0.510	5.570	0.106	7.45	133.3	2.6
720	7.656	0.0076	0.4670	0.0068	0.746	5.452	0.090	10.81	130.6	2.24
850	6.924	0.0054	0.4171	0.0051	1.133	5.366	0.100	16.54	128.6	2.4
980	6.969	0.0058	0.5320	0.0072	1.087	5.311	0.095	15.87	127.3	2.3
1050	6.643	0.0046	0.5592	0.0132	1.152	5.326	0.090	16.82	127.7	2.2
1100	7.114	0.0064	0.6690	0.0173	0.957	5.280	0.098	13.98	126.6	2.4
1150	6.594	0.0043	1.0728	0.0329	0.539	5.417	0.160	7.87	129.8	3.7
1200	6.707	0.0049	1.8633	0.0855	0.222	5.448	0.240	3.24	130.5	5.9
1250	7.473	0.0082	2.3015	0.1297	0.145	5.2858	0.110	2.12	149.6	3.2
1300	7.724	0.0090	1.3965	0.1107	0.059	5.189	0.440	0.86	146.9	12.6
Plateau age: 129.3 ± 1.6 Ma; Sample mass: 200 mg										
TR-53 whole rock, $J = 0.0137663$										
300	9.001	0.0131	0.3996	0.0089	0.261	5.151	0.180	1.02	123.6	4.3
500	7.727	0.0086	0.2170	0.0044	0.806	5.192	0.060	3.15	124.6	1.4
620	8.403	0.0095	0.1333	0.0024	1.919	5.612	0.028	7.50	134.3	0.7
720	7.605	0.0072	0.1163	0.0018	2.820	5.482	0.024	11.02	131.3	0.6
850	6.778	0.0050	0.1066	0.0013	4.345	5.317	0.026	16.98	127.5	0.6
980	7.027	0.0057	0.1386	0.0019	4.089	5.353	0.025	15.98	128.3	0.6
1050	6.730	0.0045	0.1274	0.0036	4.314	5.394	0.024	16.86	129.2	0.6
1100	7.441	0.0070	0.1335	0.0045	3.649	5.363	0.027	14.26	128.5	0.6
1150	6.458	0.0035	0.2315	0.0092	1.940	5.435	0.040	7.58	130.2	1.0
1200	6.708	0.0044	0.3596	0.0229	0.829	5.440	0.070	3.24	130.3	1.6
1250	7.501	0.0078	0.6409	0.0475	0.399	5.267	0.040	1.56	149.1	1.2
1300	7.723	0.0087	0.3708	0.0259	0.217	5.192	0.120	0.85	147.0	3.4
Plateau age: 129.7 ± 0.6 Ma; Sample mass: 200 mg										

intermontane basins (e.g., Zhang et al., 2012; Li et al., 2013a; Wu et al., 2014).

In the western Qinling orogenic belt, the magmatic activity is characterized by extensive late Triassic intrusive rocks and minor Mesozoic–Cenozoic volcanic rocks in the Elashan, Langmusi-Caibaoshan, Laozanggou-Duofutun-Hongqiang, and Baiguan-Haoti areas (e.g., Qinghai BGMR, 1991; Yu et al., 2001; Feng et al., 2003). Our study focuses on the volcanic rocks in the Laozanggou-Duofuntun area, especially on the intermediate to acidic lavas (Fig. 1b, c). These volcanic rocks are considered to occur in the continental-facies volcanic-sedimentary package of the Duofutun Group, which is composed of sandstone, carbonaceous slate and intermediate-acid volcanic rocks (Li et al., 2013c). The Laozanggou volcanic sequence has a total thickness of more than 2000 m and is uncomfortably underlain by the Middle Triassic Gulangti Group and overlain by Paleogene–Neogene red-beds (Fig. 1c). Its lower segment consists of basalt, pyroxene andesite and andesite, tuff and volcanic breccia, and the upper segment mainly of intermediate to acid lava and volcanic breccia.

The andesitic and dacitic samples in this study are from the middle–upper segment of the Laozanggou volcanic sequence (Fig. 1b, c). They are little altered apart from minor chloritization and kaolinization of phenocrysts. Their mineral assemblages contain 25%–45% phenocrysts and 40%–60% matrix, with phenocrysts being of 20%–30% plagioclase, 0–15% clinopyroxene and 0–5% biotite and the fine-grained groundmass of plagioclase, clinopyroxene and minor opaque oxides (Fig. 2a–d). Our andesitic samples display a hyalopilitic texture and have subhedral plagioclase (25–35 vol.%) and clinopyroxene (5–12 vol.%) phenocrysts and minor biotite (0–3 vol.%) phenocryst (Fig. 2a–c). Subhedral plagioclase and clinopyroxene can be up to 5 mm and 2 mm in size, respectively. Most plagioclase phenocryst show crossed twinning and several exhibit oscillatory zoning and simple twinning. Hornblende is only present in a few samples. Dacitic samples have from ~25 to 45 vol.% subhedral to euhedral plagioclase grains ranging from ~2 to 6 mm (Fig. 2d). The plagioclase grains have cores surrounded by the spongy zones or straight, curved/irregular margins with the matrix. Biotite is present, ranging from nearly fresh to oxidize (opacitized). Groundmass is glassy and contains microlites of plagioclase and Fe–Ti oxides.

3. Analytical methods

Hornblende grains for $^{40}Ar/^{39}Ar$ step-heating and zircon grains for U–Pb dating were separated by conventional heavy liquid and magnetic techniques, and then handpicked under a binocular microscope. The $^{40}Ar/^{39}Ar$ step-heating measurements were carried out using gas source the mass spectrometer RGA-10, at the Guangzhou Institute of Geochemistry (GIG), the Chinese Academy of Sciences (CAS), China. Correction factors for interfering argon isotopes derived from Ca and K are: $(^{38}Ar/^{36}Ar)_{Ca} = 0.1869$, $(^{38}Ar/^{37}Ar)_{Ca} = 0$, $(^{36}Ar/^{37}Ar)_{Ca} = 2.69 \times 10^{-4}$, $(^{39}Ar/^{37}Ar)_{Ca} = 7.09 \times 10^{-4}$, $(^{40}Ar/^{39}K)_k = 0.00165$. The blank of $^{40}Ar/^{36}Ar$ is 295.5. The internal standard biotite ZBH-2506 monitor yielded the age of 132.7 ± 1.2 Ma. The detailed analytical techniques follow Sang et al.

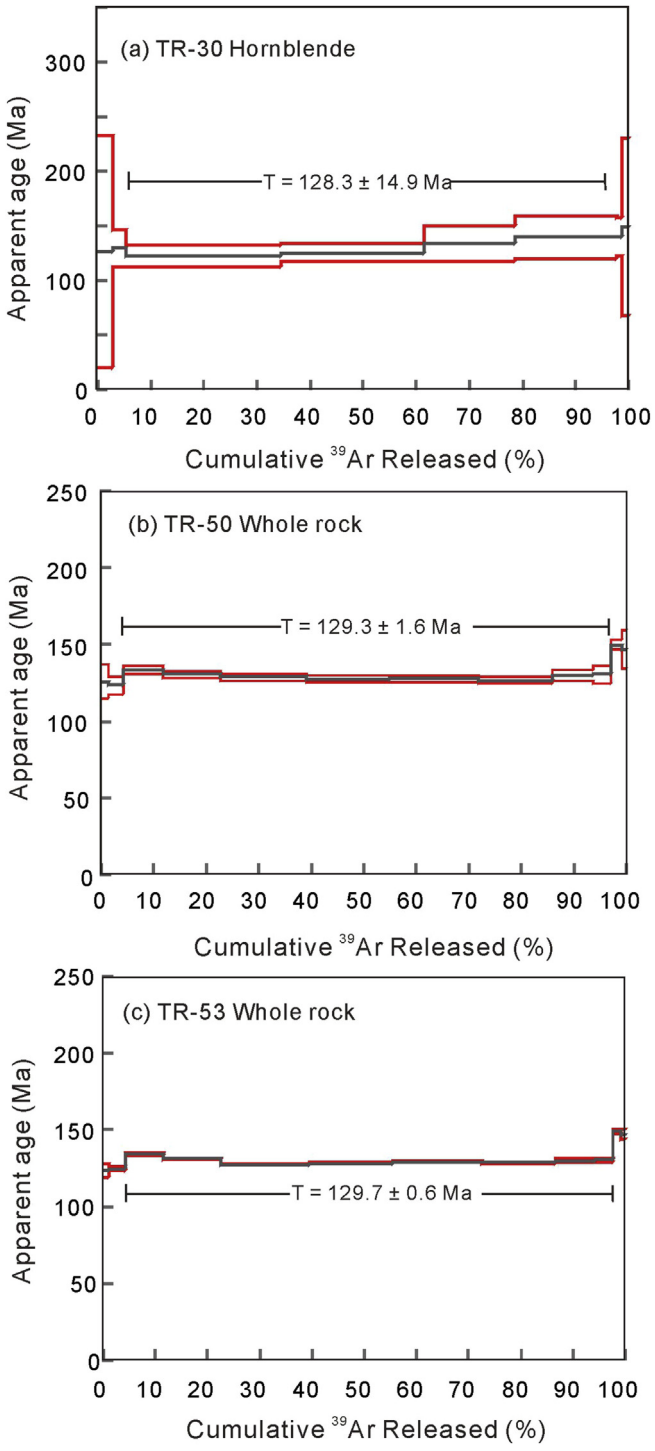

Figure 3. The $^{40}Ar/^{39}Ar$ age spectra for three andesitic samples from the early Cretaceous Laozanggou volcanic sequence in the western Qinling orogenic belt. (a) Hornblende grains from sample TR-30, (b) whole-rock sample TR-50, and (c) whole-rock sample TR-53. See Fig. 1c for sampling locations.

(1996). The $^{40}Ar/^{39}Ar$ dating results were calculated and plotted using the ArArCALC software (Koppers, 2002).

Laser ablation ICPMS (LA-ICPMS) zircon U–Pb analyses were carried out at the State Key Laboratory of Continental Dynamics, Northwest University (China), using Agilient 7500a quadruple (Q)-ICPMS attached with a Geolas laser-ablation system equipped with a 193 nm Ar-F-excimer laser. Analyses were performed under a beam diameter of ca. 30 μm and a repetition rate of 6 Hz, which yielded a signal intensity of 0.03 V for ^{238}U for the standard zircon 91500. Typical ablation time was 40 s for each measurement, resulting in pit depths of 30–40 μm. The instrumental setting and detailed analytical procedure are described by Yuan et al. (2004).

Eleven samples were crushed into 200-mesh using an agate mill for major oxide, trace elemental and Sr–Nd isotopic analyses at the GIG, CAS, China. The major oxides were analyzed by a wavelength X-ray fluorescence spectrometry with relative standard derivations of <5%. The procedures details were described by Li et al. (2005). The trace element analyses were performed on a Perkin–Elmer Sciex ELAN 6000 ICP-MS, following the procedures described by Li et al. (2002b). The Sr and Nd isotopic ratios were measured using a mass-spectrometer. The sample preparation and chemical separation are similar to those described by Wei et al. (2002) and Liang et al. (2003). The total procedure blanks were in the range of 200–500 pg for Sr and ≤50 pg for Nd. The mass fractionation corrections for Sr and Nd isotopic ratios are based on $^{86}Sr/^{88}Sr = 0.1194$ and $^{146}Nd/^{144}Nd = 0.7219$, respectively. The measured $^{87}Sr/^{86}Sr$ ratios of the (NIST) SRM987 standard and $^{143}Nd/^{144}Nd$ ratios of the La Jolla standard are 0.710265 ± 12 (2σ) and 0.511862 ± 10 (2σ), respectively.

4. Results

4.1. Ar–Ar dating and zircon U–Pb geochronological results

Three representative andesitic samples were selected for $^{40}Ar/^{39}Ar$ dating with their sampling locations and analytical results given in Fig. 1 and Table 1, respectively. The corresponding age spectra are shown in Fig. 3a–c. The hornblende grains separated from sample TR-30 yield the $^{40}Ar/^{39}Ar$ apparent ages of 123.5–140.2 Ma and a plateau age of 128.3 ± 14.9 Ma with >90% ^{39}Ar released at five successive temperature steps (Fig. 3a). Whole-rock sample TR-50 gives $^{40}Ar/^{39}Ar$ apparent ages of 127.3–133.3 Ma from the third to tenth heating steps, yielding a whole rock plateau age of 129.3 ± 1.6 Ma defined by 93% released gas (Fig. 3b). Whole-rock sample TR-53 defines a plateau age of 129.7 ± 0.6 Ma with 93% released gas at successive eight heating-steps (Fig. 3c), similar to TR-30 and TR-50.

Sample TR-53 is additionally selected for laser zircon U–Pb dating and the measured results are listed in Table 2 and shown in Fig. 4. The zircons are light brown or brown, prismatic and transparent to subtransparent in morphology, mostly euhedral and up to 100–300 μm in length with ~2:1–4:1 of length/width ratio. These zircons show well-developed oscillatory zoning in Fig. 4a, typical of igneous grains. Twelve spots on 12 grains give Th/U ratios from 0.44 to 1.19 and yield the $^{206}Pb/^{238}U$ apparent ages of 127.8–133.1 Ma with a weighted mean age of 131.3 ± 1.3 Ma (MSWD = 0.47). This age (131.3 ± 1.3 Ma) is similar, within error, to the Ar–Ar plateau age of 129.7 ± 0.6 Ma, representing the crystallization age of the TR-53 (andesite). As a result, the Ar–Ar plateau ages are considered reliable and the age of 128–131 Ma can be interpreted as the eruption age of the Laozanggou continental andesitic–dacitic sequence in the western Qinling belt, indicating an early Cretaceous origin.

4.2. Elemental and Sr–Nd isotopic geochemistry

The analytical results for major oxides, trace elements and Sr–Nd isotopic composition of the representative samples are listed in Table 3 and shown in Figs. 5–9.

SiO_2 contents for the volcanic rocks range from 56.86 wt.% to 66.86 wt.% (volatile-free), FeO^T from 5.04 wt.% to 7.58 wt.%, TiO_2 from 0.56 wt.% to 0.74 wt.%, P_2O_5 from 0.12 wt.% to 0.16 wt.%, and

Table 2
LA-ICPMS zircon U–Pb dating results for representative andesitic sample (TR-53) from the western Qinling orogenic belt.

Spot	U (ppm)	Th (ppm)	Th/U	Isotopic ratios						Apparent age (Ma)						
				$^{207}Pb/^{206}Pb$	$\pm1\sigma$	$^{207}Pb/^{235}U$	$\pm1\sigma$	$^{206}Pb/^{238}U$	$\pm1\sigma$	$^{207}Pb/^{206}Pb$	$\pm1\sigma$	$^{207}Pb/^{235}U$	$\pm1\sigma$	$^{206}Pb/^{238}U$	$\pm1\sigma$	Disc
TR-53-01	88	99	0.88	0.05574	0.00238	0.15390	0.00512	0.02002	0.00035	442	92	145	5	128	2	113
TR-53-02	213	439	0.49	0.05332	0.00207	0.15340	0.00432	0.02086	0.00036	343	85	145	4	133	2	109
TR-53-03	477	508	0.94	0.04858	0.00169	0.13776	0.00308	0.02056	0.00034	128	80	131	3	131	2	100
TR-53-04	155	131	1.19	0.05250	0.00189	0.14857	0.00359	0.02052	0.00034	307	80	141	3	131	2	108
TR-53-05	157	177	0.89	0.05206	0.00236	0.14893	0.00537	0.02075	0.00037	288	100	141	5	132	2	107
TR-53-06	145	231	0.63	0.04928	0.00219	0.14062	0.00492	0.02069	0.00036	161	101	134	4	132	2	102
TR-53-07	137	120	1.14	0.04804	0.00236	0.13754	0.00556	0.02076	0.00038	101	112	131	5	132	2	99
TR-53-08	157	186	0.85	0.05019	0.00194	0.14181	0.00390	0.02049	0.00035	204	87	135	3	131	2	102
TR-53-09	185	326	0.57	0.05111	0.00209	0.14667	0.00448	0.02081	0.00036	246	92	139	4	133	2	105
TR-53-10	220	307	0.72	0.05113	0.00208	0.14428	0.00434	0.02046	0.00035	247	91	137	4	131	2	105
TR-53-11	102	110	0.92	0.04854	0.00201	0.13927	0.00432	0.02080	0.00036	126	94	132	4	133	2	99
TR-53-12	174	391	0.44	0.05581	0.00240	0.15656	0.00517	0.02034	0.00036	445	93	148	5	130	2	112
Weighted mean age = 131.3 ± 1.3 Ma, n = 12, MSWD = 0.47																

Al_2O_3 from 15.73 wt.% to 19.09 wt.%. The analyzed samples show a calc-alkaline composition with K_2O of 0.99–2.46 wt.% (Table 3 and Fig. 5a). On the TAS diagram (Fig. 5b), these samples mainly fall into the andesitic field with the exception of TR-35 and TR-41 plotting as dacite. A similar distribution occurs on the Nb/Y–Zr/TiO_2 diagram (not shown). MgO contents for the andesitic rocks range from 2.18 wt.% to 4.67 wt.% with Mg# (Mg# = 100 × Mg/(Mg + ∑Fe) in atomic ratio) in the range of 42–56, higher than those of two dacitic samples (MgO = 1.03 wt.% and 1.06 wt.% and Mg# = 28 and 26, respectively). On Harker variation diagrams, SiO_2 increases with decreasing TiO_2, MgO, CaO and CaO/Al_2O_3 (Fig. 6a–g) but increasing Na_2O (Fig. 6h). SiO_2 is positively correlated with Nb, La and Th, and negatively correlated with Sr (Fig. 7a–d).

These volcanic samples show similar chondrite-normalized rare earth element (REE) patterns (Fig. 8a), characterized by strong enrichment in light rare earth elements (LREE), with $(La/Yb)_N$ of 7.05–17.85 and negative Eu anomalies (Eu^*/Eu = 0.64–0.82). Heavy rare earth element (HREE)-patterns are generally flat with $(Gd/Yb)_N$ ratios ranging from 1.55 to 2.38. Primitive mantle-normalized multi-elemental spidergrams are characterized by marked enrichment in LILE, depletion in Nb, Ta, P and Ti and insignificant Zr–Hf negative anomalies, with additional negative Ba anomalies (Fig. 8b). Initial Sr and Nd isotopic composition for six representative samples were back-calculated to the eruption age of ~130 Ma. Their initial $^{87}Sr/^{86}Sr$ ratios range from 0.7112 to 0.7149 and $\varepsilon_{Nd}(t)$ values from −10.2 to −6.3, similar with those of the late Triassic andesites erupted in the nearby area (Fig. 9a; Li et al., 2013a).

5. Discussion

5.1. Magma process

The high loss on ignition (LOI) of 2.06–5.77 wt.% suggests that these volcanic rocks might have been subjected to a small degree of low-temperature alteration (Wang et al., 2005). However, there is poor correlation of LOI with Rb, Sr, Zr, Nb contents and Sr–Nd isotopic composition (not shown). Such characteristics, along with the similar REE- and PM-normalized patterns (Fig. 8), suggest minimal low-temperature alteration.

Our samples defined the significant correlation of SiO_2 with other major oxides and trace elements (Figs. 6 and 7), reflective of significant fractional crystallization during magma evolution. Increasing SiO_2 and decreasing Cr and Ni with decreasing MgO (Figs. 6a and 7e–f) indicate significant fractionation crystallization of olivine and clinopyroxene (e.g., Wang et al., 2006; Xie et al., 2007). Clinopyroxene fractionation is further supported by the negative correlation of SiO_2 with CaO and CaO/Al_2O_3 (Fig. 6c and g). Their high Al_2O_3 (15.73–19.09 wt.%) and Sr (123–286 ppm)

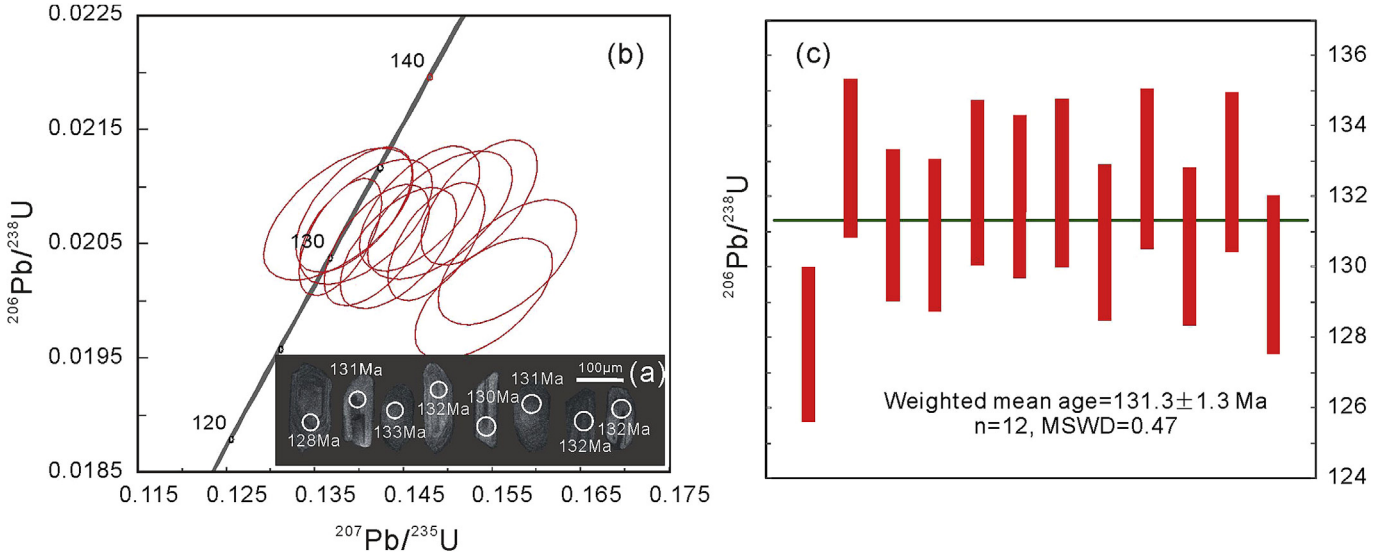

Figure 4. Concordia diagram of zircon U–Pb data for sample TR-53 from the early Cretaceous Laozanggou volcanic sequence in the western Qinling orogenic belt. Inset in (a) note the representative CL images for zircons from the sample TR-53.

Table 3
Elemental and Sr–Nd isotopic data of early Cretaceous andesite–dacite from western Qinling orogenic belt (major composition in wt.% and trace composition in ppm).

Sample	TR-30	TR-32	TR-35	TR-41	TR-44	TR-47	TR-49	TR-50	TR-53	TR-58	TR-60
SiO_2	59.12	57.53	62.97	63.47	58.22	58.34	55.59	55.60	59.41	56.54	55.40
TiO_2	0.61	0.59	0.55	0.53	0.70	0.69	0.68	0.72	0.65	0.69	0.70
Al_2O_3	17.24	16.87	16.06	14.93	17.39	16.41	17.44	17.35	18.58	17.48	18.23
Fe_2O_3	2.12	2.27	4.40	2.90	2.12	3.75	2.92	2.76	2.53	3.31	2.44
FeO	2.90	3.00	3.40	2.35	3.45	3.20	3.90	4.15	2.85	3.30	3.05
CaO	5.84	7.37	3.89	4.83	6.90	6.72	7.89	8.48	6.06	7.81	9.12
MgO	3.31	2.75	1.58	0.98	2.44	4.13	4.54	4.45	2.73	3.26	2.08
K_2O	1.64	0.93	1.55	2.31	2.37	2.17	1.78	1.65	2.22	1.88	1.80
Na_2O	2.36	2.54	2.48	2.45	2.32	2.06	2.18	2.35	2.47	2.29	2.47
P_2O_5	0.13	0.14	0.13	0.12	0.15	0.14	0.12	0.14	0.13	0.13	0.13
MnO	0.07	0.10	0.05	0.06	0.09	0.11	0.12	0.13	0.09	0.07	0.09
LOI	4.47	5.77	2.76	4.91	3.67	2.11	2.66	2.06	2.11	3.04	4.32
Mg#	55	50	28	26	45	53	56	55	49	48	42
P	472	506	495	466	553	535	430	530	450	478	519
Sc	15.9	15.9	11.5	10.5	19.1	19.5	22.5	21.8	16.1	21.0	17.4
V	63.8	65.0	22.3	33.0	77.5	82.1	103	100	55.8	98.0	90.0
Cr	115	101	11.0	39.0	188	190	184	178	32.0	169	164
Co	16.3	16.5	13.8	13.7	19.5	23.6	26.3	27.7	15.0	23.6	21.0
Ni	25.7	23.1	5.9	24.7	34.2	36.6	53.5	62.2	8.9	54.5	57.6
Cu	20.7	14.8	10.8	14.5	41.3	23.6	69.2	34.9	14.1	39.2	33.3
Ga	20.5	19.5	20.3	18.1	20.5	19.1	18.7	18.9	20.7	18.8	20.0
Rb	69.4	37.8	69.2	85.4	103.2	91.5	80.3	68.9	91.0	83.7	82.4
Sr	254	233	197	123	276	282	250	272	286	282	273
Y	18.2	17.7	27.5	18.5	20.6	20.6	19.8	19.7	20.0	19.0	20.9
Zr	130	131	158	151	158	134	125	130	139	131	143
Nb	8.96	9.41	10.4	10.70	9.77	9.20	7.02	8.13	8.66	7.52	8.18
Ba	353	125	446	502	431	383	327	301	471	380	357
La	26.3	26.4	54.0	38.3	28.1	25.0	19.9	20.2	25.2	19.8	24.1
Ce	52.1	52.6	105.9	76.0	55.8	50.0	40.5	40.7	49.8	41.1	46.7
Pr	6.17	6.15	12.4	8.83	6.58	5.91	4.88	4.83	5.80	4.92	5.72
Nd	23.3	23.0	44.8	32.5	24.7	22.4	18.8	18.7	22.3	18.4	21.8
Sm	4.54	4.42	7.88	5.75	4.88	4.50	3.99	3.95	4.31	3.89	4.30
Eu	1.09	1.04	1.84	1.06	1.10	1.03	1.01	1.01	1.09	0.98	1.06
Gd	3.70	3.57	6.50	4.43	4.26	4.10	3.80	3.84	3.90	3.63	3.94
Tb	0.59	0.58	1.01	0.67	0.70	0.64	0.61	0.61	0.63	0.61	0.64
Dy	3.24	3.17	5.38	3.55	3.77	3.78	3.51	3.51	3.59	3.43	3.71
Ho	0.64	0.65	1.02	0.65	0.77	0.75	0.73	0.72	0.73	0.69	0.76
Er	1.79	1.76	2.67	1.73	2.11	2.05	2.02	1.98	2.05	1.95	2.05
Tm	0.28	0.27	0.40	0.26	0.34	0.33	0.32	0.32	0.33	0.31	0.33
Yb	1.70	1.64	2.35	1.54	2.09	2.01	2.03	1.97	2.06	1.91	2.01
Lu	0.27	0.26	0.36	0.24	0.33	0.32	0.32	0.31	0.32	0.29	0.31
Hf	3.51	3.29	4.17	3.94	3.98	3.54	3.34	3.35	3.64	3.31	3.78
Ta	0.58	0.59	0.64	0.66	0.61	0.57	0.44	0.49	0.55	0.44	0.51
Th	9.27	9.12	9.84	12.2	10.07	8.76	6.31	6.06	8.66	6.40	8.60
U	2.39	2.29	2.30	2.36	2.28	2.09	1.49	1.46	2.00	1.55	2.13
$(La/Yb)_N$	11.1	11.5	16.5	17.9	9.65	8.93	7.05	7.34	8.78	7.42	8.60
$(Gd/Yb)_N$	1.80	1.80	2.29	2.38	1.69	1.69	1.55	1.61	1.57	1.57	1.63
Eu*	0.81	0.80	0.78	0.64	0.73	0.73	0.80	0.79	0.82	0.80	0.78
$^{87}Rb/^{86}Sr$			1.02		1.08	0.94	0.93	0.73		0.73	
$^{147}Sm/^{144}Nd$			0.11		0.12	0.12	0.13	0.13		0.13	
$^{87}Sr/^{86}Sr$			0.7144		0.7169	0.7162	0.7137	0.7126		0.7133	
2σ			17		17	19	17	17		17	
$^{143}Nd/^{144}Nd$			0.5120		0.5121	0.5121	0.5121	0.5123		0.5121	
2σ			9		11	12	13	12		13	
$(^{87}Sr/^{86}Sr)_i$			0.7125		0.7149	0.7145	0.7116	0.7113		0.7117	
$\varepsilon_{Nd}(t)$			−10.2		−8.6	−8.6	−8.7	−6.3		−9.1	
T_{DM} (Ga)			1.57		1.65	1.68	1.80	1.58		1.83	

Note: Mg# = 100 × Mg/(Mg + Fe^T). The initial isotopic ratios are back-calculated to 130 Ma.

contents, along with weak Sr and Eu negative anomalies (Fig. 8a,b), reflect minor plagioclase fractionation. The negative correlation between SiO_2 and TiO_2 (Fig. 6f) and depletion in Ti shown in Fig. 8b might be related to the Ti–Fe-oxides fractionation, but the apatite fractionation might be insignificant due to the relatively constant P_2O_5 contents irrespective of SiO_2 (Fig. 6e). However, the fractional crystallization of these minerals (e.g., olivine and clinopyroxene) cannot explain the variations of the incompatible element and Sr–Nd isotopic ratios. Such characteristics suggest the involvement of crustal components either in magma source or by crustal assimilation en route (e.g., DePaolo, 1981).

Our samples have high $(^{87}Sr/^{86}Sr)_i$ and low $\varepsilon_{Nd}(t)$ values, suggestive of the involvement of crustal components. Their $\varepsilon_{Nd}(t)$ values and Nb/La ratios decrease with increasing SiO_2 contents, indicating the processes of crustal assimilation or assimilated fractional crystallization during magma ascend (Fig. 10; Fan et al., 2010). This is further supported by their low Nb/La ratios, ranging from 0.19 to 0.40, and the samples with higher SiO_2 contents (~65 wt.%) and lower Mg# (~27) (e.g., dacites TR-35 and TR-41), which exhibit the lower Nd isotopic values (~−10.2). Available data show that, in the western Qinling orogenic belt, the Precambrian basement is poorly exposed and related geochemical data are scarce due to the

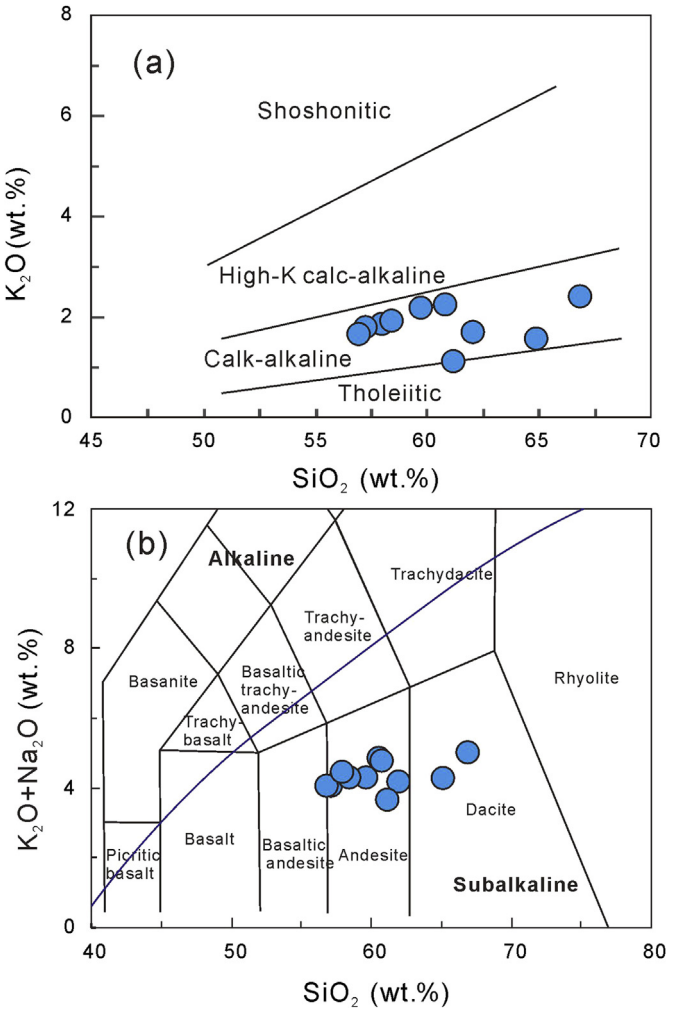

Figure 5. The classification diagram of SiO_2 and (a) K_2O (after Peccerillo and Taylor, 1976) and (b) $K_2O + Na_2O$ (after Middlemost, 1994) for the early Cretaceous Laozanggou volcanic sequence in the western Qinling orogenic belt.

Phanerozoic sedimentary coverage. Thus, the Wudangshan Group in the eastern Qinling orogenic belt, consisting mainly of the Neoproterozoic basaltic–dacitic–rhyolitic and sedimentary rocks, are usually considered to have tectonic affinity with the Precambrian basement of the western Qinling orogenic belt (e.g., Ling et al., 2008, 2010; Dong et al., 2017). However, the Wudangshan volcanic rocks have wide SiO_2 variation ranging from 44 wt.% to 80 wt.% (Ling et al., 2002) and ε_{Nd} (t = 130 Ma) values from −2.7 to +1.7. This indicates that the derivation of the Wudangshan Precambrian basement should have more complex rock-association and more depleted Nd isotopic composition, in contrast to those of the Laozanggou intermediate-acidic volcanic rocks.

Magma mixing of mantle- and lower crust-derived melts can also be ruled out based on the Sr–Nd modeling calculations. The Mesozoic ultramafic–mafic rocks and diorites from the Jianzha, Xiekeng and Wumei areas in the western Qinling orogenic belt are believed to be derived from an enriched lithospheric mantle, and could be used as the mantle end-member for the Laozanggou intermediate-acidic volcanic samples. The Wudangshan Group is herein proposed as the representative of the crustal end-member. Our observations show that the mixing of the lithosphere- and crust-derived magmas have higher $(^{87}Sr/^{86}Sr)_i$ ratios, and lower $\varepsilon_{Nd}(t)$ and MgO contents than the Laozanggou intermediate-acidic volcanic samples (Fig. 8a; Luo et al., 2012, 2015; Li et al., 2014). The magma mixing of lower crust- and upper crust-derived components is an alternative for producing the Laozanggou volcanic rocks. However, a simple mixing calculation yields an unrealistic mixing proportion up to 20%–40% for the western Qinling upper crust. As a result, the binary magma mixing model is rejected.

5.2. Magma source nature

Samples TR-49 and TR-50 have the lowest SiO_2 contents and $(^{87}Sr/^{86}Sr)_i$ ratios but the highest MgO, Mg#, and $\varepsilon_{Nd}(t)$ values (−6.3) of all analyzed samples, which can be regarded as the representatives of the least-contaminated rocks. Their elemental and isotopic compositions could be close to those of the primary magma. Thus, the primary magma of the Laozanggou volcanic rocks might be calc-alkaline magma and characterized by high Mg# (~56) and $\varepsilon_{Nd}(t)$ value (~−6.3), but low SiO_2 contents (~56 wt.%) and $(^{87}Sr/^{86}Sr)_i$ ratio (~0.7112), along with enrichment in LILE and depletion in HFSE with pronounced Nb–Ta negative anomalies (Fig. 8b).

Samples TR-49 and TR-50 have high La/Nb (2.5–2.8), Ba/Nb (37.1–46.7) and Zr/Nb (16.0–17.8) ratios and Nb–Ta and Ti negative anomalies (Fig. 8b), similar to arc-like volcanic rocks (Stern, 2002). The subduction-modified mantle wedge might be a plausible magma source for these volcanic rocks. However, there is no geological evidence for supporting the development of the early Cretaceous subduction event in the study area. In contrast, evidence shows that the oceanic subduction in the region ceased no later than the Triassic. Thus, the metasomatized mantle wedge might be ancient rather than newly-formed. The Mesoproterozoic Nd model ages for TR-49 and TR-50 also suggest that the source experienced LILE and LREE enrichment during an “older” metasomatic event. Available data show that the Guanzizhen mafic-intermediate igneous rocks in a western Qinling orogenic belt formed in a Late Cambrian to Early Ordovician island-arc setting and are characterized by the geochemical signatures of a depleted source (e.g., Pei et al., 2007; Dong et al., 2011a,b). Such features suggest that the subduction-related metasomatism of the mantle source beneath the western Qinling orogenic belt should occur after the Early Ordovician. As a result, the enriched elemental and isotopic signatures for the Laozanggou volcanic rocks were most likely developed by the Triassic subduction/collision in the Qinling orogenic belt. In fact, the Triassic diorites from the Xiekeng, Jianzha and Wumei areas are considered to be derived from lithospheric mantle, highly-modified by subduction-related fluids/melts, and are characterized by high LILE enrichment, HFSE depletion, enriched Sr–Nd isotopic composition, and are geochemically similar to the Laozanggou volcanic sequence (Luo et al., 2012, 2015; Li et al., 2014).

Magmas that originate from a slab-metasomatized source generally show high Sr contents and La/Yb ratios with depleted Sr–Nd compositions, which contradict to our observation from the Laozanggou volcanic sequence. A more likely explanation is that their source is characterized by enriched lithosphere modified by the subduction − sediments with high $(^{87}Sr/^{86}Sr)_i$ ratios and low $\varepsilon_{Nd}(t)$ values (e.g., Oxburgh and Turcotte, 1968). Magma from a recycled sediment-modified source is commonly characterized by low Sr/Ce (<5) and Sr/Y ratios (e.g., Chauvel et al., 1995; Kapenda et al., 1998; Shimoda et al., 1998; Tatsumi, 2001, 2006). Our samples have high Sr/Ce (>6) and Sr/Y ratios, indicating that the metasomatism of the sediment-derived melt was unlikely to be the dominant metasomatic agent. Instead, their high Ba/La and Rb/Sr ratios support the involvement of sediment-released fluid. Thus, the magma source of the Laozanggou volcanic rocks might be an enriched lithosphere previously (possibly in the Triassic) modified by the recycled sediment-derived fluid beneath the

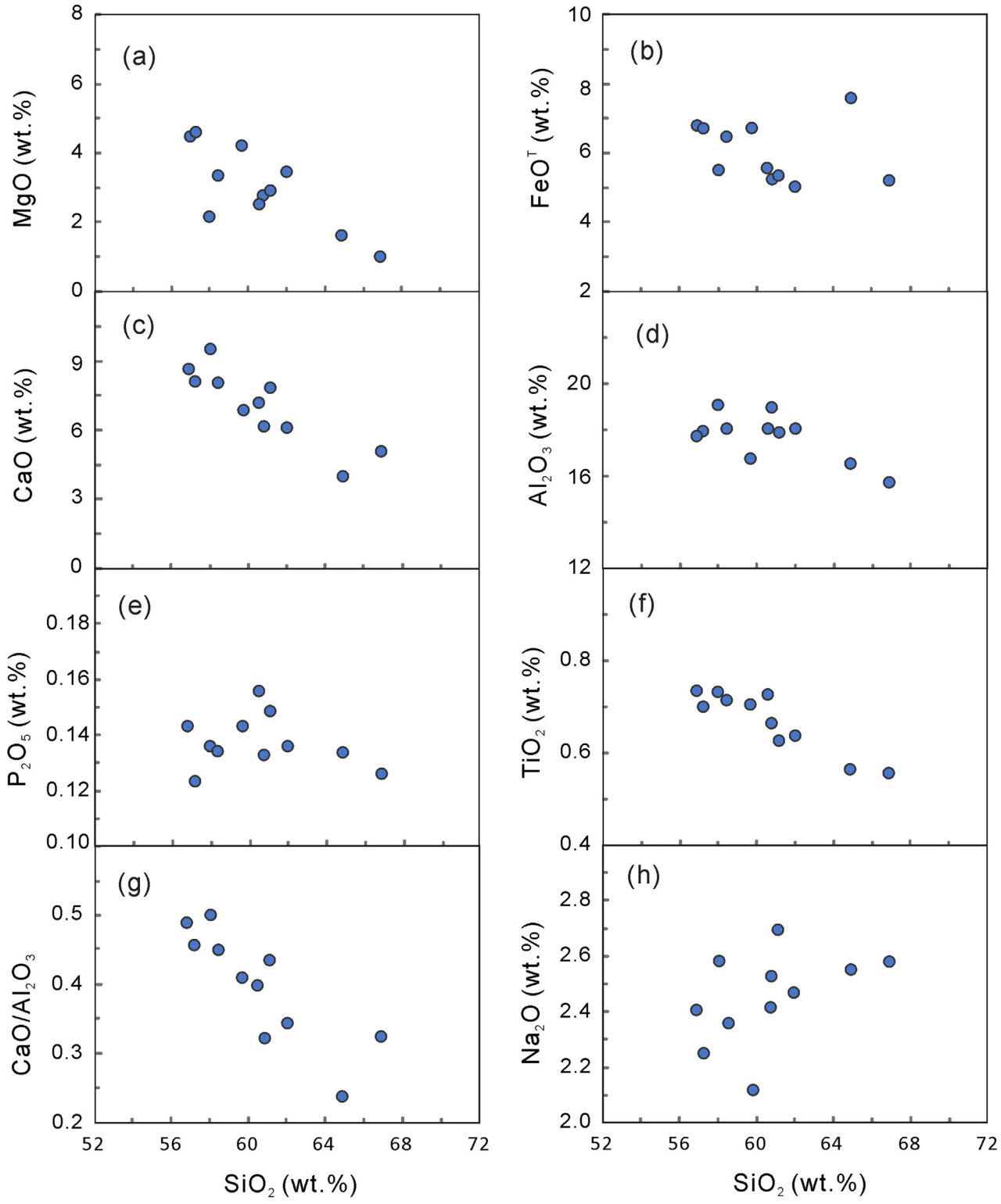

Figure 6. SiO_2 versus major oxides and CaO/Al_2O_3 for the early Cretaceous Laozanggou volcanic sequence in the western Qinling orogenic belt. The major oxides are normalized to 100 wt.%.

western Qinling orogenic belt. For the Laozanggou volcanic rocks, they could be generated as the result of (1) mantle-derived melt with crustal assimilation or assimilated fractional crystallization (AFC) processes; (2) partial melting of lower/middle continental crust; and (3) mixing of mantle- and crust-derived melts (e.g., Defant and Drummond, 1990; Foley, 1992; Rapp and Watson, 1995; Borg and Clynne, 1999; Fan et al., 2004). As mentioned above, our data queries the possibility of case (2) and (3). Thus, the Laozanggou andesites and dacites are most likely the AFC products of primary magma represented by samples TR-49 and TR-50.

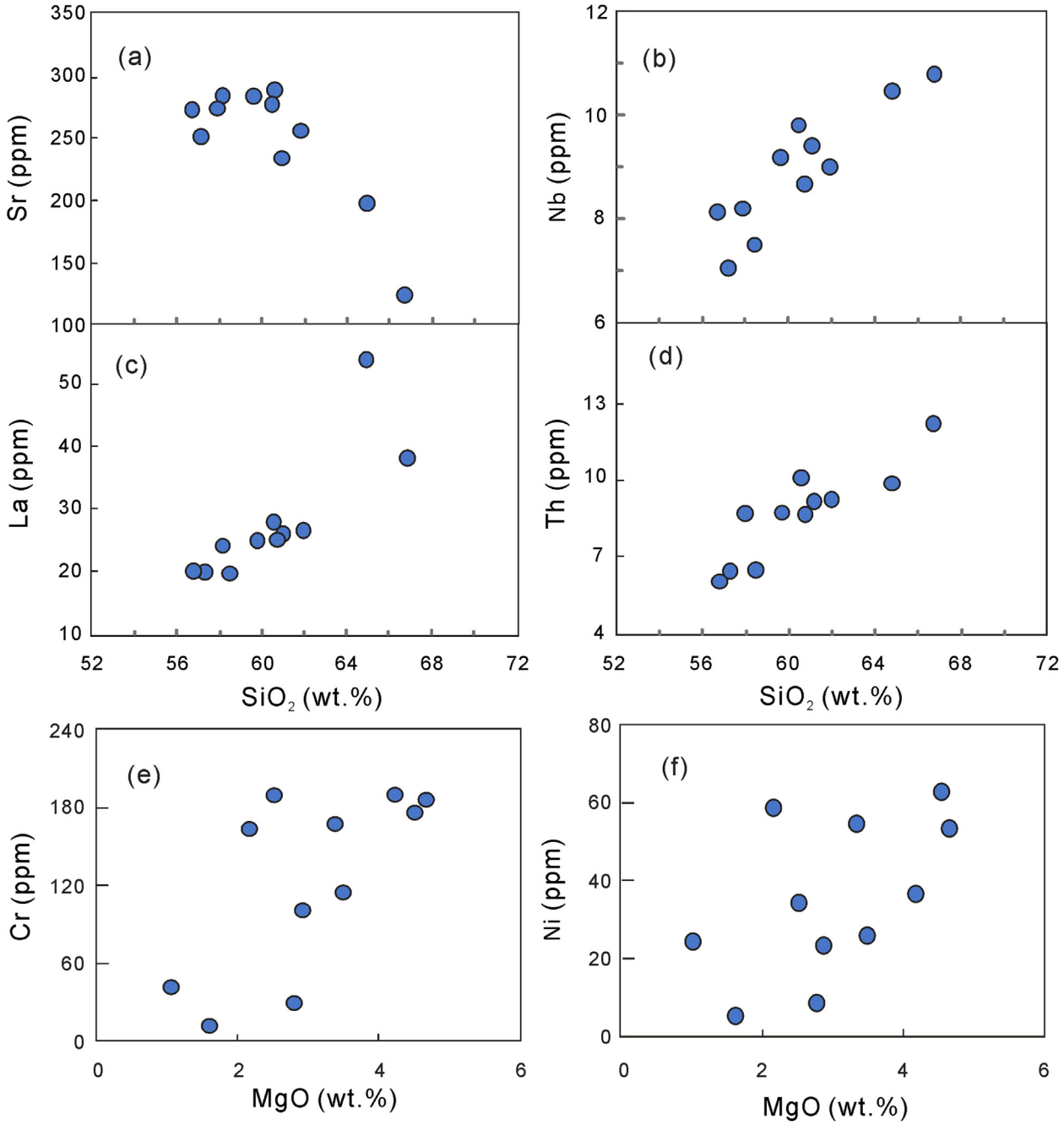

Figure 7. Variations of SiO_2 and trace elements, and MgO versus Cr and Ni for the early Cretaceous Laozanggou volcanic sequence in the western Qinling orogenic belt.

Our modeling results, as shown in Fig. 9b, further indicate that the assimilation of 10%–15% crustal component is required to be added into the primary magma for balancing the elemental and Sr–Nd isotopic signatures of the other Laozanggou volcanic samples.

5.3. Tectonic implication

Our geochronological and geochemical data indicate that the Laozanggou intermediate-acidic volcanic rocks from the Duofutun Group erupted at 128–131 Ma. These volcanic rocks have typical calc-alkaline geochemical characteristics and derived from a previously-modified enriched mantle. Available data show that the early Cretaceous (112–103 Ma) basaltic rocks from the adjacent Duofutun, Duohemao and Hongqiang areas belong to alkaline rocks and originated from asthenospheric mantle with the proportional input of a delaminated lithospheric component (e.g., Ding et al., 2013; Li et al., 2013b; Zhang et al., 2018). Such geochemical change from ~130 Ma andesites–dacites to ~110 Ma basalts reflects a shift in the source from the enriched lithospheric to asthenospheric mantle. Hawkesworth and Gallagher (1993) believed that this change of the mantle source from relatively shallow to deep level with time might be related to the lithosphere thinning in the intracontinental tectonic setting.

Question remains as to which petrogenetic mechanism triggered the lithospheric thinning for inducing the eruption of the early Cretaceous intracontinental volcanic rocks in the western Qinling orogenic belt. An upwelling mantle plume and its interaction with

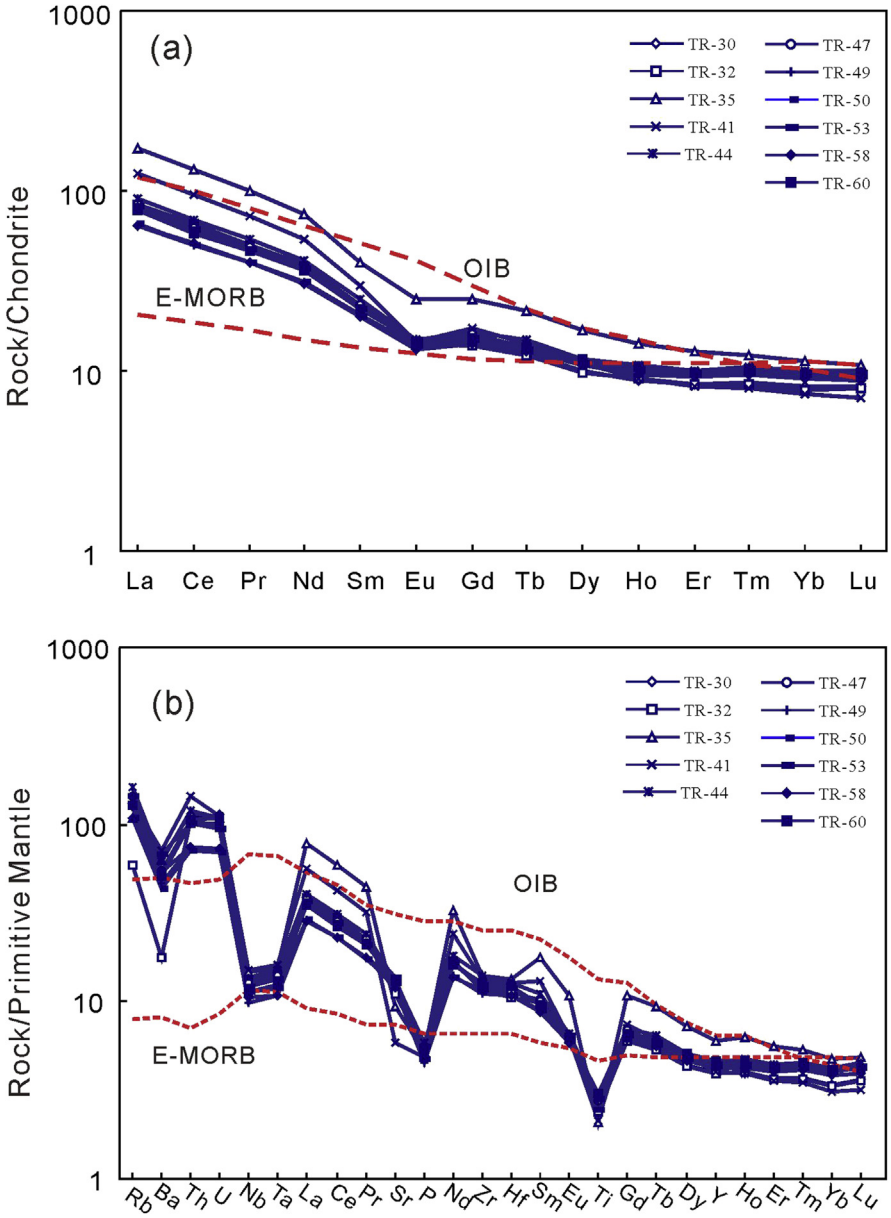

Figure 8. (a) Chondrite-normalized rare-earth elements patterns and (b) primitive mantle-normalized spidergrams for the early Cretaceous Laozanggou volcanic sequence in the western Qinling orogenic belt. Chondrite- and primitive mantle-normalize values are from Taylor and McLennan (1985) and Sun and McDonough (1989), respectively. Data for OIB (Oceanic-island basalt) and E-MORB (enriched mid-ocean ridge basalt) are from Sun and McDonough (1989).

the lithosphere can provide the possibility for magma generation. However, our geochemical data from the early Cretaceous volcanic rocks argue against a plume-derived magma (Campbell, 2005; Elkins-Tanton, 2005; Campbell and Davies, 2006). In addition, the Late Mesozoic hotspot track and related geological evidence are not obvious in the western Qinling orogenic belt.

Regional extension is another possible mechanism for inducing the lithospheric thinning to generate the Early Cretaceous volcanic rocks. In the Qinling orogenic belt, the orientation of regional extension changed from NW–SE in the early Cretaceous to NE–SW-in the late Cretaceous (e.g., Ratschbacher et al., 2003). Dai et al. (2014) and Li et al. (2013b, 2015) argued that the 101–112 Ma alkali basalts in the western Qinling orogenic belt were generated in a post-collisional setting in response to the lithospheric extension. The mafic dikes intruded along W–E trending intermontane basin in the western Qinling orogenic belt are dated at 107 ± 1 Ma and 103 ± 4 Ma (Craddock et al., 2012; Li et al., 2013a), suggesting late Early Cretaceous (<110 Ma) intracontinental extension. However, our Laozanggou intermediate-acidic volcanic rocks erupted at ~130 Ma, older than the time of the lithospheric thinning of the western Qinling orogenic belt.

The detachment of the lithospheric root (e.g., Hawkesworth et al., 1995; Molnar et al., 1998; Hoernle et al., 2006) might be an alternative model for the formation of the Laozanggou volcanic rocks in the western Qinling orogenic belt. This model requires a gravitationally unstable lithospheric mantle in response to the shortening of the continental lithosphere (e.g., Molnar et al., 1998; Schott et al., 2000). During the late Jurassic to early Cretaceous (prior to the eruption of the Laozanggou volcanic rocks), the whole Qinling region underwent transpressive shortening, evidenced by the large scale of folding and faulting, and the angular unconformity between the upper Cretaceous and the underlying package

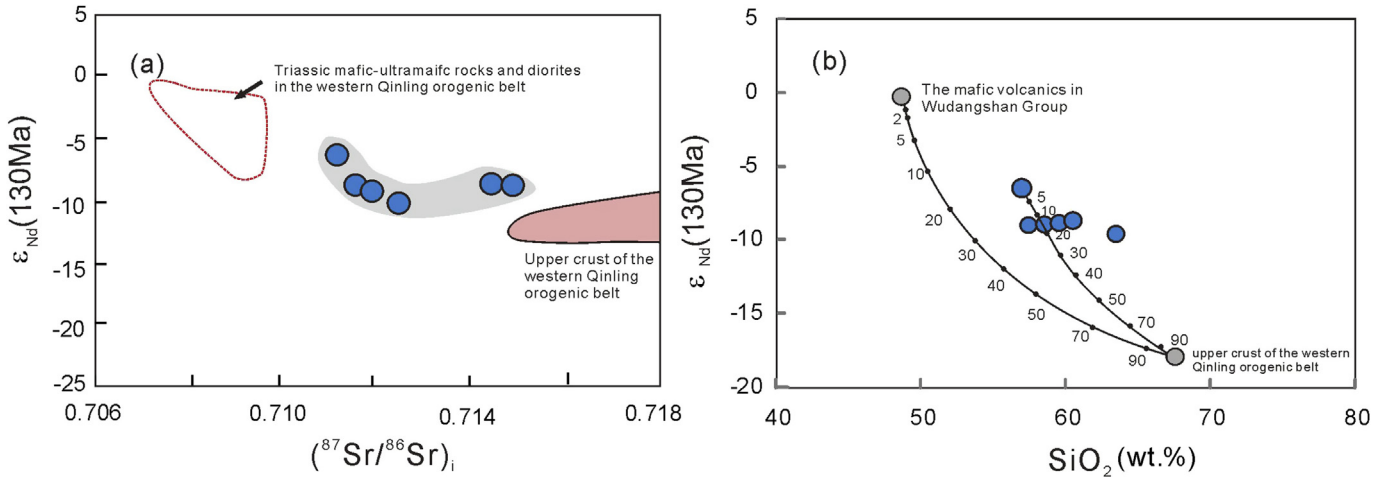

Figure 9. (a) Initial $^{87}Sr/^{86}Sr(t)$ versus $\varepsilon_{Nd}(t)$ (t = 130 Ma) for the early Cretaceous Laozanggou volcanic sequence in the western Qinling orogenic belt. Data for the Triassic mafic–ultramafic rocks and diorites in the western Qinling are from Li et al. (2014) and Luo et al. (2012, 2015). Data of the upper crust in the western Qinling orogenic belt are from Chen et al. (2008). (b) Modeling calculation of SiO_2 (in wt.%) vs. $\varepsilon_{Nd}(t)$ for the crustal assimilation en route for the early Cretaceous Laozanggou andesitic–dacitic volcanic sequence in the western Qinling orogenic belt. Data for the mafic volcanic rocks from the Wudangshan Group and the upper crust in the western Qinling orogenic belt are from Ling et al. (2002) and Chen et al. (2008), respectively.

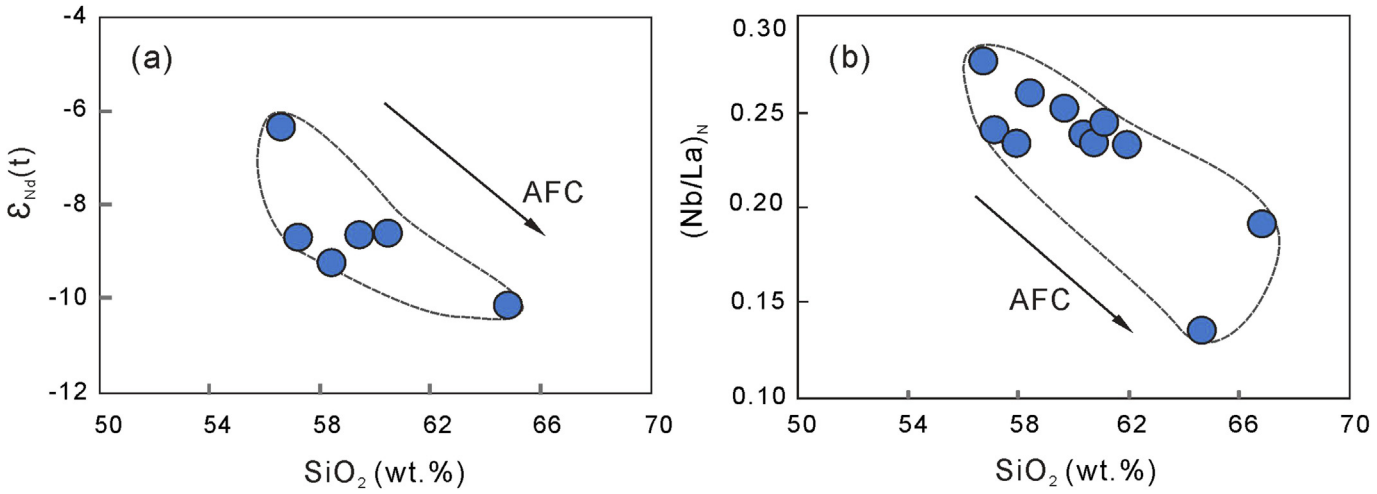

Figure 10. SiO_2 versus $\varepsilon_{Nd}(t)$ (a) and $(Nb/La)_N$ (b) for the early Cretaceous Laozanggou volcanic sequence in the western Qinling orogenic belt. Abbreviation: AFC, assimilation and fractional crystallization.

(e.g., Qinghai BGMR, 1991; Dong et al., 2011a, 2016; Li et al., 2013a; Wu et al., 2014; Dong and Santosh, 2016). Following the late Jurassic–early Cretaceous crustal shortening, the removal of the lithospheric root promotes asthenospheric upwelling resulting in tectonic reactivation and lithospheric thinning (e.g., Gao et al., 2004; Hoernle et al., 2006). In such a situation, the uprising of lithospheric thermal boundary resulted in partial melting of the previously (possibly Triassic) subduction-modified enriched mantle to generate the early Cretaceous Laozanggou primary magma. Fractional crystallization of this magma along with assimilation of 10%–15% crustal materials resulted the Laozanggou intermediate-acidic volcanic rocks. This was followed by the generation of the asthenosphere-derived alkali basalts at ~110 Ma in response to ongoing upwelling of the asthenospheric mantle.

Acknowledgment

We would like to thank Dr. X.Y. Li and L.Y. Fan for their help during fieldwork and geochemical analyses. This work is financially supported by National Natural Science Foundation of China (Grant Nos. 41421002, 41302176 and 41872236), National Basic Research Program of China (Grant No. 2014CB440901), and Foundation of Shaanxi Educational committee (14JK1760). P.A. Cawood acknowledges support from Australian Research Council (Grant FL160100168). We thank the anonymous reviewers for their thorough, critical and constructive reviews and comments.

References

Ames, L., Zhou, G.Z., Xiong, B.C., 1996. Geochronology and isotopic character of ultrahigh-pressure metamorphism with implications for collision of the Sino-Korean and Yangtze cratons, central China. Tectonics 15, 472–489.

Ayers, J.C., Dunkle, S., Gao, S., Miller, C.F., 2002. Constraints on timing of peak and retrograde metamorphism in the Dabie Shan ultrahigh-pressure metamorphic belt, east-central China, using U–Th–Pb dating of zircon and monazite. Chemical Geology 186, 315–331.

Boettcher, A.L., 1973. Volcanism and orogenic belts – the origin of andesites. Tectonophysics 17, 223–240.

Borg, L.E., Clynne, M.A., 1999. The petrogenesis of felsic calc-alkaline magmas from the southernmost Cascades, California: origin by partial melting of basaltic lower crust. Journal of Petrology 39, 1197–1222.

Bryant, D.L., Ayers, J.C., Gao, S., Miller, C.F., Zhang, H.F., 2004. Geochemical, age, and isotopic constraints on the location of the Sino-Korean/Yangtze Suture and evolution of the Northern Dabie Complex, east central China. Geological Society of America Bulletin 116, 698–717.
Campbell, I.H., 2005. Large igneous provinces and the mantle plume hypothesis. Elements 1, 265–270.
Campbell, I.H., Davies, G.F., 2006. Do mantle plumes exist? Episodes 29, 162–168.
Cawood, P.A., Hawkesworth, C.J., Dhuime, B., 2013. The continental record and the generation of the continental crust. Geological Society of America Bulletin 125, 14–32.
Chauvel, C., Goldstein, S.L., Hofmann, A.W., 1995. Hydration and dehydration of oceanic crust controls Pb evolution in the mantle. Chemical Geology 126, 65–75.
Chen, Y.L., Li, D.P., Zhou, J., Zhang, H.F., Liu, F., Nie, L.S., Jiang, L.T., Liu, X.M., 2008. U–Pb ages of zircons in Western Qinling Mountain, China, and their tectonic implication. Earth Science Frontiers 15 (4), 88–107 (in Chinese with English abstract).
Chiaradia, M., Muntener, O., Beate, B., 2011. Enriched basaltic andesites from mid-crustal fractional crystallization, recharge, and assimilation (Pilavo volcano, western Cordillera of Ecuador). Journal of Petrology 52, 1107–1141.
Craddock, W.H., Kirby, E., Zhen, D.W., Liu, J.H., 2012. Tectonic setting of Cretaceous basins on the NE Tibetan Plateau: insights from the Jungong basin. Basin Research 24, 51–69.
Dai, L.Q., Zhao, Z.F., Zheng, Y.F., 2014. Geochemical insights into the role of metasomatic hornblendite in generating alkali basalts. Geochemistry, Geophysics, Geosystems 15, 3762–3779.
Davies, J.W., Stevenson, D.J., 1992. Physical model of source region of subduction zone volcanic. Journal of Geophysical Research 97, 2037–2070.
Defant, M.J., Drummond, M.S., 1990. Derivation of some modern arc magmas by melting of young subducted lithosphere. Nature 347 (6294), 662–665.
DePaolo, D.J., 1981. Trace element and isotopic effects of combined wall rock assimilation and fractional crystallization. Earth and Planetary Science Letters 53, 189–202.
Ding, Y., Yu, X.H., Mo, X.X., Li, X.W., Huang, X.F., Wei, P., 2013. Geochronology, geochemistry and petrogenesis of the Hongqiang basalts from Northeast Qinghai–Tibetan plateau. Earth Science Frontiers 20, 180–191 (in Chinese with English abstract).
Dong, Y.P., Zhang, G.W., Zhao, X., Yao, A.P., Liu, X.M., 2004. Geochemistry of the subduction-related magmatic rocks in the Dahong Mountains, northern Hubei Province: constraint on the existence and subduction of the eastern Mianlue oceanic basin. Science China Series D. Earth Sciences 47, 366–377.
Dong, Y.P., Zhang, G.W., Neubauer, F., Liu, X.M., Genser, J., Hauzenberger, C., 2011a. Tectonic evolution of the Qinling orogen, China: review and synthesis. Journal of Asian Earth Sciences 41, 213–237.
Dong, Y.P., Zhang, G.W., Hauzenberger, C., Neubauer, F., Yang, Z., Liu, X.M., 2011b. Palaeozoic tectonics and evolutionary history of the Qinling orogen: evidence from geochemistry and geochronology of ophiolite and related volcanic rocks. Lithos 122, 39–56.
Dong, Y.P., Sun, S.S., Yang, Z., Liu, X.M., Zhang, F.F., Li, W., Cheng, B., He, D.F., Zhang, G.W., 2017. Neoproterozoic subduction-accretionary tectonics of the south Qinling belt, China. Precambrian Research 293, 73–90.
Dong, Y.P., Yang, Z., Liu, X.M., Sun, S.S., Li, W., Cheng, B., Zhang, F.F., Zhang, X.N., He, D.F., Zhang, G.W., 2016. Mesozoic intracontinental orogeny in the Qinling mountains, central China. Gondwana Research 30, 144–158.
Dong, Y.P., Santosh, M., 2016. Tectonic architecture and multiple orogeny of the Qinling orogenic belt, Central China. Gondwana Research 29, 1–40.
Elkins-Tanton, L.T., 2005. Continental magmatism caused by lithospheric delamination. In: Foulger, G.R., Natland, J.H., Presnall, D.C., Anderson, D.L. (Eds.), Plates, Plumes, and Paradigms, Geological Society of America Special Paper, vol. 388. Geological Society of America, pp. 449–461.
Enkin, R.J., Yang, Z., Chen, Y., Courtillot, V., 1992. Paleomagnetic constraints on the geodynamic history of the major blocks of China from Permian to the present. Journal of Geophysical Research 97, 13953–13989.
Ernst, W.G., 2010. Subduction-zone metamorphism, calc-alkaline magmatism, and convergent-margin crustal evolution. Gondwana Research 18, 8–16.
Fan, W.M., Guo, F., Wang, Y.J., Zhang, M., 2004. Late Mesozoic volcanism in the northern Huaiyang tectono-magmatic belt, central China: partial melts from a lithospheric mantle with subducted continental crust relicts beneath the Dabie Orogen? Chemical Geology 209 (1–2), 27–48.
Fan, W.M., Wang, Y.J., Zhang, A.M., Zhang, F.F., Zhang, Y.Z., 2010. Permian arc-back arc basin development along the Ailaoshan tectonic zone: geochemical, isotopic and geochronological evidence from the Mojiang volcanic rocks, Southwest China. Lithos 119 (3–4), 553–568.
Feng, Y.M., Cao, X.Z., Zhang, E.P., 2003. Geological evolution of the western Qinling orogen. Northwestern Geology 36, 1–1214 (in Chinese with English abstract).
Feng, Y.M., Gao, X.Z., Zhang, E.P., Hu, Y.X., Pan, X.P., Yang, J.L., Jia, Q.Z., Li, W.M., 2002. Structure, Orogenic Processes and Geodynamic of the Western Qinling Orogen. Xi'an Map Press, Xi'an, pp. 1–263 (in Chinese).
Foley, S.F., 1992. Petrological characterization of the source components of potassic magmas: geochemical and experimental constraints. Lithos 28, 187–204.
Gao, S., Rudnick, R.L., Yuan, H.L., Liu, X.M., Liu, Y.S., Xu, W.L., Ling, W.L., Ayers, J., Wang, X.C., Wang, Q.H., 2004. Recycling lower continental crust in the North China Craton. Nature 432, 892–897.
Gill, J.B., 1981. Orogenic Andesites and Plate Tectonics. Springer, Berlin, p. 390.
Grove, T.L., Kinzler, R.J., 1986. Petrogenesis of andesites. Annual Review of Earth and Planetary Sciences 14, 417–454.
Hacker, B.R., Ratschbacher, L.W., Ireland, L., Walker, D., Dong, S., 1998. U/Pb zircon ages constrain the architecture of the ultrahigh-pressure Qinling–Dabie Orogen, China. Earth and Planetary Science Letters 161, 215–230.
Hawkesworth, C.J., Gallagher, K., 1993. Mantle hotspots, plume and regional tectonics as causes of intraplate magmatism. Terra Nova 5, 552–559.
Hawkesworth, C.J., Gallagher, K., Hergt, J.M., McDermott, F., 1993. Mantle and slab contributions in arc magmas. Annual Review of Earth and Planetary Sciences 21, 175–204.
Hawkesworth, C., Turner, S., Gallagher, K., Hunter, A., Bradshaw, T., Rogers, N., 1995. Calc-alkaline magmatism, lithospheric thinning and extension in the basin and range. Journal of Geophysical Research 100, 10271–10286.
Hoernle, K., White, J.D.L., van den Bogaard, P., Hauff, F., Coombs, D.S., Werner, R., Timm, C., GarbeSchönberg, D., Reay, A., Cooper, A.F., 2006. Cenozoic intraplate volcanism on New Zealand: upwelling induced by lithospheric removal. Earth and Planetary Science Letters 248, 350–367. https://doi.org/10.1016/j.epsl.2006.06.001.
Jahn, B.M., Wu, F.Y., Lo, C.H., Tsai, C.H., 1999. Crust–mantle interaction induced by deep subduction of the continental crust: geochemical and Sr–Nd isotopic evidence from post-collisional mafic–ultramafic intrusions of the northern Dabie complex, central China. Chemical Geology 157, 119–146.
Kapenda, D., Kampunzu, A.B., Canabis, B., Namegabe, M., Tshimanga, K., 1998. Petrology and geochemistry of post-kinematic mafic rocks from the Palaeoproterozoic Ubendian belt, NE Katanga (DRC). Geologische Rundschau 87, 345–362.
Kelemen, P.B., Yogodzinski, G.M., School, D.W., 2003. Along-strike variation in the Aleutian Island arc: genesis of high Mg# andesite and implications for continental crust. Geophysical Monograph Series 138, 223–276.
Koppers, A.A.P., 2002. ArAR CALC – software for 40Ar/39Ar age calculations. Computers & Geosciences 28, 605–619.
Kröner, A., Zhang, G.W., Zhuo, D.W., Sun, Y., 1993. Granulites in the Tongbai area, Qinling belt, China: geochemistry, petrology, single zircon geochronology and implications for tectonic evolution of eastern Asia. Tectonics 12, 245–255.
Lee, C.-T.A., Morton, D.M., Kistler, R.W., Baird, A.K., 2007. Petrology and tectonics of Phanerozoic continent formation: from island arcs to accretion and continental arc magmatism. Earth and Planetary Science Letters 263, 370–387.
Li, S.G., Huang, F., Li, H., 2002a. Post-collisional lithosphere delamination of Dabie-Sulu orogen. Chinese Science Bulletin 47, 259–263.
Li, W., Dong, Y.P., Guo, A.L., Liu, X.M., Liu, Y.Q., Zha, X.F., Zhang, K.L., 2013a. Sedimentary fill history of the Huicheng Basin in the west Qinling mountains and associated constraints on Mesozoic intracontinental tectonic evolution. Science China Series D. Earth Sciences 43 (5), 730–744.
Li, S.G., Sun, W.D., Zhang, G.W., 1996. Chronology and geochemistry of metavolcanic rocks from Heigouxia valley in Mian-Lue tectonic belt, South Qinling: evidence for a Paleozoic oceanic basin and its close time. Science China Series D. Earth Sciences 39, 300–310.
Li, S.G., Xiao, Y.L., Liou, D.L., Chen, Y.Z., Ge, N.J., Zhang, Z.Q., Sun, S.S., Zhang, R.Y., Hart, S.R., Wang, S.S., 1993. Collision of the north China and Yangtze blocks and formation of coesite-bearing eclogites: timing and processes. Chemical Geology 109, 89–111.
Li, X.H., Li, Z.X., Zhou, H., Liu, Y., Kinny, P.D., 2002b. U–Pb zircon geochronology, geochemistry and Nd isotopic study of Neoproterozoic bimodal volcanic rocks in the Kangdian Rift of South China: implications for the initial rifting of Rodinia. Precambrian Research 113 (1–2), 135–154.
Li, X.H., Su, L., Chung, S.L., Li, Z.X., Liu, Y., Song, B., Liu, D.Y., 2005. Formation of the Jinchuan ultramafic intrusion and the world's third largest Ni–Cu sulfide deposit: associated with the ~825 Ma south China mantle plume? Geochemistry, Geophysics, Geosystems 6, Q11004. https://doi.org/10.1029/2005GC001006.
Li, X.W., Mo, X.X., Yu, X.H., Ding, Y., Huang, X.F., Wei, P., He, W.Y., 2013b. Geochronological, geochemical and Sr–Nd–Hf isotopic constraints on the origin of the Cretaceous intraplate volcanism in West Qinling, Central China: implications for asthenosphere–lithosphere interaction. Lithos 177, 381–401.
Li, X.W., Mo, X.X., Yu, X.H., Ding, Y., Huang, X.F., Wei, P., He, W.Y., 2013c. Petrology and geochemistry of the early Mesozoic pyroxene andesites in the Maixiu area, west Qinling, China: products of subduction or syn-collision? Lithos 172, 158–174.
Li, X.W., Li, J., Bader, T.M., Mo, X.X., Scheltens, M., Chen, Z.Y., Xu, J.F., Yu, X.H., Huang, X.F., 2015. Evidence for crustal contamination in intra-continental OIB-like basalts from West Qinling, central China: a Re–Os perspective. Journal of Asian Earth Sciences 98, 436–445.
Li, X.W., Mo, X.X., Bader, T., Scheltens, M., Yu, X.H., Dong, G.C., Huang, X.F., 2014. Petrology, geochemistry and geochronology of the magmatic suite from the Jianzha Complex, central China: petrogenesis and geodynamic implications. Journal of Asian Earth Sciences 95, 164–181.
Liang, X.R., Wei, G.J., Li, X.H., Liu, Y., 2003. Precise measurement of $^{143}Nd/^{144}Nd$ and Sm/Nd ratios using multiple-collectors inductively couple plasma–mass spectrometer (MC–ICP–MS). Geochimica 32 (1), 91–96 (in Chinese with English abstract).
Ling, W.L., Cheng, J.P., Wang, X.H., Zhou, H.W., 2002. Geochemical features of the Neoproterozoic igneous rocks from the Wudang region and their implications for the reconstruction of the Jinning tectonic evolution along the south Qinling

orogenic belt. Acta Petrologica Sinica 18, 25–36 (in Chinese with English abstract).
Ling, W.L., Ren, B.F., Duan, R.C., Liu, X.M., Mao, X.W., Peng, L.H., Liu, Z.X., Cheng, J.P., Yang, H.M., 2008. Timing of the Wudangshan, Yaolinghe volcanic sequences and mafic sills in South Qinling: U–Pb zircon geochronology and tectonic implication. Chinese Science Bulletin 53, 2192–2199.
Ling, W.L., Duan, R.C., Liu, X.M., Cheng, J.P., Mao, X.W., Peng, L.H., Liu, Z.X., Yang, H.M., Ren, B.F., 2010. U–Pb dating of detrital zircons from the Wudangshan Group in the South Qinling and its geological significance. Chinese Science Bulletin 55, 2440–2448.
Luo, B.J., Zhang, H.F., Lv, X.B., 2012. U–Pb zircon dating, geochemical and Sr–Nd–Hf isotopic compositions of Early Indosinian intrusive rocks in West Qinling, central China: petrogenesis and tectonic implications. Contributions to Mineralogy and Petrology 164, 551–569.
Luo, B.J., Zhang, H.F., Xu, W.C., Guo, L., Pan, F.B., Yang, H., 2015. The middle Triassic Meiwu Batholith, west Qinling, Central China: implications for the evolution of compositional diversity in a composite Batholith. Journal of Petrology 56, 1139–1172.
Mattauer, M., Mattle, P., Malavieille, J., Tapponnier, P., Masluski, H., Xu, Z.Q., Li, Y.L., Tang, Y.Q., 1985. Tectonics of Qinling belt: build-up and evolution of eastern Asia. Nature 317, 496–500.
Meng, Q.R., Qu, H.J., Hu, J.M., 2007. Triassic deep-marine sedimentation in the western Qinling and Songpan terrane. Science China Series D. Earth Sciences 246–263.
Meng, Q.R., Wang, E., Hu, J.M., 2005. Mesozoic sedimentary evolution of the northwest Sichuan basin: implication for continued clockwise rotation of the South China block. Geological Society of America Bulletin 117, 396–410.
Meng, Q.R., Zhang, G.W., 2000. Geologic framework and tectonic evolution of the Qinling Orogen, Central China. Tectonophysics 323, 183–196.
Middlemost, E.A.K., 1994. Naming materials in the magma/igneous rock system. Earth-Science Reviews 37, 215–224.
Miyashiro, A., 1974. Volcanic rock series in island arcs and active continental margins. American Journal of Science 274, 321–355.
Molnar, P., Houseman, G.A., Conrad, C., 1998. Rayleigh–Taylor instability and convective thinning of mechanically thickened lithosphere: effects of nonlinear viscosity decreasing exponentially with depth and of horizontal shortening of the layer. Geophysical Journal International 133, 568–584.
Okay, A.I., Sengör, A.M.C., 1993. Tectonics of an ultra-high pressure metamorphic terrane: the Dabie Shan/Tongbai Shan orogen, China. Tectonics 12, 1320–1334.
Oxburgh, E.R., Turcotte, D.L., 1968. Mid-ocean ridges and geotherm distribution during mantle convection. Geophysical Research 73, 2643.
Pearce, J.A., Peate, D.W., 1995. Tectonic implications of the composition of volcanic arc magmas. Annual Review of Earth and Planetary Sciences 23, 251–285.
Peccerillo, A., Taylor, S.R., 1976. Geochemistry of Eocene calc-alkaline volcanic rocks from the Kastamonu area, Northern Turkey. Contributions to Mineralogy and Petrology 58, 63–81.
Pei, X.Z., Ding, S.P., Zhang, G.W., Liu, H.B., Li, Z.C., Li, C.Y., Liu, Z.Q., Meng, Y., 2007. The LA–ICP–MS zircons U–Pb ages and geochemistry of the Baihua basic igneous complexes in Tianshui area of West Qinling. Science China Series D. Earth Sciences 50, 264–276.
Poli, S., Schmidt, M.W., 2002. Petrology of subducted slabs. Annual Review of Earth and Planetary Sciences 30, 207–235.
Qinghai BGMR (Qinghai Bureau of Geology and Mineral Resources), 1991. Regional Geology of Qinghai Province. Geology Publishing House, Beijing, p. 662 (in Chinese).
Rapp, R.P., Watson, E.B., 1995. Dehydration melting of metabasalt at 8–32 kbar: implications for continental growth and crust–mantle recycling. Journal of Petrology 36, 891–931.
Ratschbacher, L., Hacker, B.R., Calvert, A., Webb, L.E., Grimmer, J.C., McWilliams, M.O., Ireland, T., Dong, S., Hu, J., 2003. Tectonics of the Qinling (Central China): tectonostratigraphy, geochronology, and deformation history. Tectonophysics 366, 1–53.
Reubi, O., Blundy, J., 2009. A dearth of intermediate melts at subduction zone volcanoes and the petrogenesis of arc andesites. Nature 461, 1269–1273.
Rudnick, R., Gao, S., 2003. Composition of the continental crust. In: Rudnick, R. (Ed.), The Crust: Treatise on Geochemistry. Elsevier, Amsterdam, pp. 1–64.
Sang, H.Q., Wang, S.S., Qiu, J., 1996. The ^{40}Ar–^{39}Ar ages of pyroxene, hornblende and plagioclase in Taipingzhai granulites in Qianxi County, Hebei Province and their geological implications. Acta Petrologica Sinica 12 (4), 390–400 (in Chinese with English abstract).
Schott, B., Yuen, D.A., Schmeling, H., 2000. The significance of shear heating in continental delamination. Physics of the Earth and Planetary Interiors 118, 273–290.
Sengör, A.M.C., 1985. East Asian tectonic collage. Nature 318, 16–17.
Shellnutt, J.G., Belousov, A., Belousova, M., Wang, K.L., Zellmer, G.F., 2014. Generation of calc-alkaline andesite of the Tatun volcanic group (Taiwan) within an extensional environment by crystal fractionation. International Geology Review 56, 1156–1171.
Shimoda, G., Tatsumi, Y., Nohda, S., Ishizaka, K., Jahn, B.M., 1998. Setouchi high-Mg andesites revisited; geochemical evidence for melting of subducting sediments. Earth and Planetary Science Letters 160, 479–492.
Stern, R.J., 2002. Subduction zones. Reviews of Geophysics 40 (4), 1–38.
Sun, S.S., McDonough, W.F., 1989. Chemical and isotopic systematics of oceanic basalts: implications for mantle composition and processes. In: Saunders, A.D., Norry, M.J. (Eds.), Magmatism in the Ocean Basins, Special Publications, vol. 42. Geological Society, London, pp. 313–345.
Tatsumi, Y., 2001. Geochemical modeling of partial melting of subducting sediments and subsequent melt–mantle interaction: generation of high-Mg andesites in the Setouchi volcanic belt, southwest Japan. Geology 29, 323–326.
Tatsumi, Y., 2006. High-Mg andesites in the Setouchi volcanic belt, southwestern Japan: analogy to Archean magmatism and continental crust formation? Annual Review of Earth and Planetary Sciences 34, 467–499.
Taylor, S.R., McLennan, S.M., 1985. The Continental Crust: Its Composition and Evolution. Blackwell Scientific Publications, Oxford, p. 312.
Till, C.B., Grove, T.L., Withers, A.C., 2012. The beginnings of hydrous mantle wedge melting. Contributions to Mineralogy and Petrology 163, 669–688.
Wang, Q., Wyman, D.A., Xu, J.F., Zhao, Z.H., Jian, P., Xiong, X.L., Bao, Z.W., Li, C.F., Bai, Z.H., 2006. Petrogenesis of Cretaceous adakitic and shoshonitic igneous rocks in the Luzong area, Anhui Province (eastern China): implications for geodynamics and Cu–Au mineralization. Lithos 89, 424–446.
Wang, Y.J., Fan, W.M., Peng, T.P., Zhang, H.F., Guo, F., 2005. Nature of the Mesozoic lithospheric mantle and tectonic decoupling beneath the Dabie Orogen, Central China: evidence from $^{40}Ar/^{39}Ar$ geochronology, elemental and Sr–Nd–Pb isotopic compositions of Early Cretaceous mafic igneous rocks. Chemical Geology 220, 165–189.
Wei, G.J., Liang, X.R., Li, X.H., Liu, Y., 2002. Precise measurement of Sr isotopic composition of liquid and solid base using (LP) MC–ICPMS. Geochimica 31, 295–299.
Wilson, M., 1989. Igneous Petrogenesis. Oxford University Press, Oxford, p. 466.
Wu, G.L., Meng, Q.R., Duan, L., Li, L., 2014. Early Mesozoic structural evolution of the eastern West Qinling, northwest China. Tectonophysics 630, 9–20.
Xie, Z., Li, Q.Z., Chen, J.F., Gao, T.S., 2007. The geochemical characteristics of the early Cretaceous volcanics in the Luzong region and their source significances. Geological Journal of China Universities 13, 235–245 (in Chinese with English abstract).
Yu, X.H., Mo, X.X., Liao, Z.L., Zhao, X., Su, Q., 2001. Temperature and pressure condition of garnet lherzolite and websterite from west Qinling. Science in China Series D. Earth Sciences 44, 155–161.
Yuan, H.L., Gao, S., Liu, X.M., Li, H.M., Gunther, D., Wu, F.Y., 2004. Accurate U–Pb age and trace element determinations of zircon by laser ablation inductively coupled plasma mass spectrometry. Geostandards and Geoanalytical Research 28, 353–370.
Zellmer, G.F., Annen, C., Charlier, B.L.A., George, R.M.M., Turner, S.P., Hawkesworth, C.J., 2005. Magma evolution and ascent at volcanic arcs: constraining petrogenetic processes through rates and chronologies. Journal of Volcanology and Geothermal Research 140, 171–191.
Zhai, X.M., Day, H.W., Hacker, B.R., You, Z.D., 1998. Paleozoic metamorphism in the Qinling orogen, Tongbai mountains, central China. Geology 26, 371–374.
Zhang, F.F., Wang, Y.J., Cawood, P.A., Dong, Y.P., 2018. Geochemistry, $^{40}Ar/^{39}Ar$ geochronology, and geodynamic implications of Early Cretaceous basalts from the western Qinling orogenic belt, China. Journal of Asian Earth Sciences 151, 62–72.
Zhang, G.W., Guo, A.L., Yao, A.P., 2004. Western Qinling-Songpan continental tectonic node in China's continental tectonics. Earth Science Frontiers 11 (3), 23–32 (in Chinese).
Zhang, G.W., Zhang, Z.Q., Dong, Y.P., 1995a. Nature of main tectono-lithostratigraphic units of the Qinling orogen: implications for the tectonic evolution. Acta Petrologica Sinica 11, 101–114 (in Chinese with English abstract).
Zhang, G.W., Meng, Q.R., Lai, S.C., 1995b. Structure and tectonics of the Qinling orogenic belt. Science in China (Series B) 38, 13–29.
Zhang, G.W., Meng, Q.R., Yu, Z.P., Sun, Y., Zhou, D.W., Guo, A.L., 1996. Orogenesis and dynamics of the Qinling orogen. Science in China Series D. Earth Sciences 39, 225–234.
Zhang, G.W., Yu, Z., Cheng, S., Li, T., Xue, F., Zhang, C., 1989. The major suture zone of the Qinling orogenic belt. Journal of Southeast Asian Earth Sciences 3, 63–76.
Zhang, G.W., Yu, Z.P., Dong, Y.P., Yao, A.P., 2000. On Precambrian framework and evolution of the Qinling belt. Acta Petrologica Sinica 16, 11–21 (in Chinese with English abstract).
Zhang, G.W., Zhang, B.R., Yuan, X.C., Chen, J.Y., 2001. Qinling Orogenic Belt and Continental Dynamics. Science Press, Beijing, pp. 1–855 (in Chinese).
Zhang, H.F., Chen, Y.L., Xu, W.C., Liu, R., Yuan, H.L., Liu, X.M., 2006. Granitoids around Gonghe basin in Qinghai province: petrogenesis and tectonic implications. Acta Petrologica Sinica 22, 2910–2922 (in Chinese with English abstract).
Zhang, J.Y., Ma, C.Q., Xiong, F.H., Liu, B., 2012. Petrogenesis and tectonic significance of the Late Permian–Middle Triassic calc-alkaline granites in the Balong region, eastern Kunlun orogen, China. Geological Magazine 149, 892–908.
Zheng, J.P., Griffin, W.L., Sun, M., O'Reilly, S.Y., Zhang, H.F., Zhou, H.W., Xiao, L., Tang, H.Y., Zhang, Z.H., 2009. Tectonic affinity of the West Qinling terrane (central China): north China or Yangtze? Tectonics 29, TC2009. https://doi.org/10.1029/2008TC002428.
Zheng, Y.F., 2008. A perspective view on ultrahigh-pressure metamorphism and continental collision in the Dabie–Sulu orogenic belt. Chinese Science Bulletin 53, 3081–3104.